ESHID-600886

Final

BASELINE DATA EVALUATION FOR SOIL VAPOR EXTRACTION AT MATERIAL DISPOSAL AREA L, SOLID WASTE MANAGEMENT UNIT 54 006, AT TECHNICAL AREA 54

Contract No.: 286642

Prepared for

LOS ALAMOS NATIONAL LABORATORY
Los Alamos, New Mexico

May 2015

Prepared by

WESTON SOLUTIONS, INC.
1400 Weston Way
West Chester, Pennsylvania 19380-1499

37309

Table of Contents

Section **Page**

1 INTRODUCTION 1
2 METHODOLOGY 1
2.1 Plume Interpolation 2
2.2 Mass Estimation 2
3 RESULTS 3
3.1 Q4FY14 Interpretations 4
3.2 Comparison with FY11 5
4 CONCLUSIONS 7
5 REFERENCES 7

List of Appendices

APPENDIX A DATA PACKAGE (provided on disk)
APPENDIX B MASS CALCULATIONS (provided on disk)
APPENDIX C ACCESSING HIDDEN FEATURES OF FIGURES 3-1 THROUGH 3-10

List of Figures

Title

Figure 3-1 Q4FY14 Interpolated vapor plume for TCA
Figure 3-2 Q4FY14 Interpolated vapor plume for TCE
Figure 3-3 Q4FY11 Interpolated vapor plume for TCA
Figure 3-4 Q3FY11 Interpolated vapor plume for TCA
Figure 3-5 Q2FY11 Interpolated vapor plume for TCA
Figure 3-6 Q1FY11 Interpolated vapor plume for TCA
Figure 3-7 Q4FY11 Interpolated vapor plume for TCE
Figure 3-8 Q3FY11 Interpolated vapor plume for TCE
Figure 3-9 Q2FY11 Interpolated vapor plume for TCE
Figure 3-10 Q1FY11 Interpolated vapor plume for TCE
Figure 3-11 Comparison of Mass Distribution by Quarter
Figure 3-12 Comparison of Mass Distribution by Isoshell and Quarter Within the Tshirege
Figure 3-13 Comparison of Q4FY14 TCA Results with FY11
Figure 3-14 Comparison of Q4FY14 TCE Results with FY11
Figure 3-15 Recent Time History of VOC Parent Compounds Within Source Areas
Figure 3-16 Recent Time History of VOC Parent Compounds Within the Inner Plume
Figure 3-17 Recent Time History of VOC Parent Compounds at Plume Margins
Figure 3-18 Recent Time History of VOC Parent Compounds Within Source Areas (log scale)
Figure 3-19 Recent Time History of VOC Parent Compounds Within the Inner Plume (log scale)
Figure 3-20 Recent Time History of VOC Parent Compounds at Plume Margins (log scale)
Figure 3-21 Recent Time History of VOC Daughter Products Within Source Areas
Figure 3-22 Recent Time History of VOC Daughter Products Within the Inner Plume
Figure 3-23 Recent Time History of VOC Daughter Products at Plume Margins
Figure 3-24 Recent Time History of VOC Daughter Products Within Source Areas (log scale)
Figure 3-25 Recent Time History of VOC Daughter Products Within the Inner Plume (log scale)
Figure 3-26 Recent Time History of VOC Daughter Products at Plume Margins (log scale)

List of Tables

Title

Table 2-1 Geologic Zone Characteristics
Table 3-1 Q4FY14 Contaminant Mass Distribution
Table 3-2 Contaminant Mass Uncertainty Analysis
Table 3-3 Comparison of Total Contaminant Mass Among Sample Rounds

List of Acronyms

1,1,1-TCA	1,1,1-trichloroethane
30x	30 times
3D	three dimensional
CME	Corrective Measures Evaluation
FY	fiscal year
kg	kilogram
LANL	Los Alamos National Laboratory
MDA L	Material Disposal Area L
NMED	New Mexico Environment Department
Q4FY14	fourth quarter of fiscal year 2014
Qbof	Otowi Member of the Bandelier tuff
Qct	Cerro Toledo interval
ROI	radius of influence
RSL	Regional Screening Level
SVE	soil vapor extraction
TA 54	Technical Area 54
Tb4	Cerros del Rio basalt
TCE	trichloroethene
VOCs	Volatile Organic Compounds

1 INTRODUCTION

The objective of this report is to present baseline estimates of the distribution and mass for both 1,1,1-trichloroethane (1,1,1-TCA) and trichloroethene (TCE) in the subsurface beneath Material Disposal Area L (MDA L) located within Technical Area 54 (TA 54) at Los Alamos National Laboratory (LANL) in Los Alamos, New Mexico. The baseline contaminant plume distributions will be compared to future interpretations that will be similarly derived from data collected during a soil vapor extraction (SVE) interim measure to be conducted in 2015 (LANL 2014, 261843). Those comparisons will be provided quarterly throughout 2015 to reveal the efficacy of the current SVE system configuration (LANL 2009, 105413) for demonstrating MDA L contaminant plume reduction. The fourth quarter of fiscal year 2014 (Q4FY14) represents the baseline estimate to which future depictions will be compared. However, this report also compares the Q4FY14 model to those derived for sampling year FY11 to illustrate changes that may have occurred during the sampling hiatus of FY12 to FY14 following submittal of the MDA L Corrective Measures Evaluation (CME) Report in 2011 (LANL 2011, 205756). Comparing the Q4FY14 model with those for FY11 also provides an indication of how representative the Q4FY14 plume data are as a baseline estimate.

Plume data variability is typical even when the plume is not significantly changing in the subsurface. In fact, the American Society for Testing and Materials (ASTM) International in its Standard Guide for Soil Gas Monitoring in the Vadose Zone notes that “soil gas monitoring does not provide repeatable quantitative information over time due primarily to the dynamic nature of phase equilibria in the vadose zone and secondarily to unavoidable inconsistencies in sampling practice.” Additionally, ASTM states: “The results of certain techniques tend to be affected by minor variations in procedure despite apparent adherence to a Standard Operating Procedure” (ASTM 2006, 110404).

Short term variability in interpolated plume mass estimates on the order of those observed in the 2011-2014 data (as reported herein) cannot be directly attributed to changes in the subsurface plume mass, and may indicate a combination of variability in factors such as sampling technique, seasonal soil moisture, interpolation assumptions (e.g. constant temperature partitioning coefficient and constant TCE+TCA plume fraction), analytical laboratory techniques, and localized borehole conditions. Therefore, it is best practice to consider several rounds of pore-gas data rather than individual sampling events when determining plume characteristics or trends. Thus, for the rest of this report, all plume masses are assumed to have some level of intrinsic variability, and we stress that large changes (>50%) to the initial baseline will be used to indicate long-term plume behavior, including future success of the ongoing soil vapor extraction system.

2 METHODOLOGY

Each of the contaminant plume interpretations presented in this report were derived using procedures established during the analysis of FY09 and FY10 data, which are detailed in Appendix E of the MDA L CME (LANL 2011, 205756) and summarized in the following subsections. Each interpretation is based on soil vapor data collected from 85 sampling ports during the respective quarters. A total of 186 ports were sampled in Q4FY14 but only the 85 previously sampled ports were used for the Q4FY14 interpretations to ensure consistency with both previous and future rounds of data collection and analysis. The one deviation from the procedure established in the CME is that the data from each quarter are currently interpreted separately whereas they were averaged in the past to smooth the temporal variability exhibited by many of the MDA L ports.

2.1 Plume Interpolation

Vapor concentrations of 1,1,1-TCA and TCE at each of the 85 sampled ports were interpolated to three dimensional (3D) representations of each compound for each quarter. Interpolation applies local trends in irregularly spaced data over short distances to fill the gaps between samples using a regular grid. The minimum tension option of the earthVision 9.0 software package (Dynamic Graphics, 2014) was used. This algorithm accounts for all data, regardless of geologic unit, in a single gridding pass so the resulting plume does not exhibit discontinuities at stratigraphic contacts. The algorithm is very fast and uses a feedback mechanism to minimize sharp changes in concentration gradient wherever possible. Various forms of kriging were evaluated but each required exhaustive spatial dependence modeling and longer calculation times. Kriging also does not provide a mechanism for mitigating extrapolation errors in the presence of minor data gaps that are inconsistent with the conceptual model of radial vapor diffusion through the dry Bandelier Tuff. The primary benefit of kriging is that it provides a means of estimating uncertainty associated with a given estimate. The minimum tension algorithm was selected over kriging due to the relative ease of application and smoother results. To estimate the uncertainty associated with the minimum tension results, a sensitivity analysis was performed in which 36 interpolations were conducted by varying the model resolution, anisotropy factor, and the exponent of the power function used to transform the data prior to interpolation (standard practice for data ranging over several orders of magnitude). The standard deviation and mean of these 36 realizations were used to derive plume distributions representing the minimum and maximum plume extents at the 95% confidence interval.

2.2 Mass Estimation

The volatile organic compounds (VOCs) detected in the unsaturated zone beneath MDA L are distributed among vapor, dissolved, and sorbed phases. Equilibrium partitioning theory, which is described in detail in the MDA L CME (LANL 2011, 205756) allows concentrations in the sorbed and dissolved phases to be derived from vapor-phase sample concentrations according to Equation 2-1. The presence of a non-aqueous liquid phase beneath MDA-L was ruled out by concentrations of VOCs that are orders of magnitude less than their respective vapor pressures. The variables in Equation 2-1 consist of both contaminant and formation properties. Contaminant-specific equilibrium constants were obtained from NMED (2009, 106420) and are supplied in the descriptions of these variables below. Strata specific properties are summarized in Table 2-1 and were obtained for the various tuff units beneath MDA L from Springer (2005, 098534) unless otherwise noted.

$$C_{bulk} = \frac{C_{air}\left(\theta_{air} + \theta_{water}/H' + \left(K_{oc}\ f_{oc}\ \rho_{soil}\right)/H'\right)}{\rho_{soil}}$$

Equation 2-1

Where:

C_{air} is the vapor-phase concentration of a VOC yielded by pore-gas monitoring.

θ_{air} is the air-filled porosity of the formation (difference between the total porosity and θ_{water}).

θ_{water} is the volumetric water content of the formation.

H' is the Henry's law constant for the VOC. 1,1,1-TCA=0.705 and TCE=0.4.

K_{oc} is the octanol-carbon distribution coefficient. 1,1,1-TCA=48.6 and TCE=107 L/kg.

f_{oc} is the fraction of organic carbon. Assumed 0.0005 globally (0.33 of the soil value in NMED, 2009).

ρ_{soil} is the bulk density, or dry mass per unit volume, of the formation.

The total mass of each contaminant was calculated by intersecting the estimates of vapor-phase plume distribution with the WC09b EarthVision 3D geologic framework model for MDA L and using the results as input to Equation 2-1. Each 3D plume was consequently discretized into numerous concentration isoshells with geologic zone information attached. The isoshells are multiples of the Tier1 screening thresholds for each contaminant established during plume analysis for the CME (LANL 2011, 205756). The volumes of each isoshell were multiplied by the average concentration for that shell, the strata-specific parameters of Table 2-1, the appropriate contaminant specific equilibrium constants, and unit conversion factors to obtain the mass of each compound in kilograms (kg). Two 125-ft cylinders representing the radius of influence (ROI) for the SVE system supplied by LANL scientists were also intersected with the plume models to facilitate evaluation of the potential SVE system impact in the future. The mass of each unique combination of contaminant, phase, isoshell, stratum, SVE zone, and sampling round were stored in a table to be integrated and visualized in various ways using pivot tables and pivot charts in Microsoft Excel.

3 RESULTS

This section includes several views of the modeled 3D vapor plume distributions for 1,1,1-TCA and TCE as well as the interpolated mass estimates derived from the combination of those distributions with the overlapping geologic framework. The Q4FY14 baseline will be discussed first and then compared with FY11 models. Mass estimates are subdivided in several ways to elaborate on differences between the 1,1,1-TCA and TCE by sampling round. The mass estimates within the footprints of the 125-ft ROIs for the current SVE system are also prepared to facilitate closer inspection of changes that might be attributed to mass removal through SVE. The two SVE wells were completed as part of a pilot study and subsequently tested to determine their ROI (LANL 2009, 105413).

All plume interpretations are presented in multi-pane figures that illustrate both plan and section views of the plumes extracted from the respective 3D models, Figures 3-1 through 3-10. These 2D views are depicted using concentration contours that are multiples of the Tier1 screening levels for the respective compounds. Both the data and the contour lines use a symbology consistent with what was used in the CME (LANL 2011, 205756). Filled contours of additional concentration isoshells are provided as supplemental information pertinent to the discussion of mass distribution. This layer can be toggled off using the layers pane within Adobe Reader and will print only when it is toggled on. There are also additional layers in the Adobe pdf containing the mean, minimum, and maximum plume distributions based on the sensitivity analysis. These are toggled off by default but are useful for illustrating the potential differences in plume distribution from what is currently considered the “best estimate.” The mass estimates from these additional simulations are discussed, but separate figures were not created.

The plan view in the upper left of each figure depicts the maximum extents and concentrations of the pertinent contaminant plume. This map also shows the locations of the three section lines used to produce the orthogonal cross-sections that surround the plan view. The cross-sections show the vertical extents of the contaminant plumes along with the majority of the data upon which the interpretations are based. Data depicted in the plan views reveal only the maximum concentrations from each borehole. Sample concentrations are not posted since the symbology reflects the concentration magnitudes and the data are provided in Appendix A. However, concentrations may be obtained directly from the figure in question using the “object data” button on the analysis toolbar within the pdf. Clicking any of the visible data points using the “object data” tool will cause a table of the sample concentrations and other attributes to appear in a new pane within the pdf.

3.1 Q4FY14 Interpretations

Figures 3-1 and 3-2 depict the baseline (Q4FY14) vapor-phase distribution of 1,1,1-TCA and TCE beneath MDA L, respectively. Elevated concentrations of both contaminants are centered on two clusters of disposal shafts within MDA L. The two SVE wells completed near each of these two source areas are superimposed on the figures along with their anticipated 125-ft ROIs. The eastern source is larger with regard to 1,1,1-TCA and western source is larger with regard to TCE. Maximum concentrations of 1,1,1-TCA are approximately 30 times (30x) the Tier1 threshold of 42,300-ug/m^3. Maximum concentrations of TCE are approximately 250x the Tier1 screening threshold of 2,000-ug/m^3. Both plumes exhibit a symmetrical oblate shape consistent with the conceptual model of radial vapor diffusion through a dry matrix. The lateral extents of the plumes are well bounded to the northwest and southeast (along transect A-A') and reasonably well bounded to the southwest. Two directional boreholes (54-01015 and 54-01016) bound the plumes to the northeast but these data were not incorporated into the interpolations. Although these boreholes were sampled in Q4FY14, they were not sampled routinely in the last several years and were therefore excluded to avoid biasing the baseline interpretations.

Both contaminant plumes are predicted to extend into the upper 100 feet of the Cerros del Rio basalt (Tb4). Elevated concentrations in the deeper ports of borehole 54-27642 are primarily responsible for the vertical extent of the 1,1,1-TCA plume. With the exception of these two ports, 1,1,1-TCA concentrations decrease rapidly at the interface of the Tshirege member of the Bandelier tuff and the underlying Cerro Toledo interval (Qct). In contrast, boreholes 54-27641 (to the west) and 54-27642 (to the east) both show TCE concentrations in excess of 25x the Tier1 threshold within Qct. However, all three of these deep boreholes show decreasing concentrations of both contaminants with depth.

Table 3-1 summarizes the mass contained in the various phases of both contaminants beneath MDA L based on the Q4FY14 plume interpretations. The interpolated mass estimates were also segregated by geology and contaminant level, in a fashion consistent with what was used in the CME, to expose several features of the plume distributions. The first item of note is that the total mass of 1,1,1-TCA (740-kg) is approximately double that of TCE (339-kg). Although maximum TCE concentrations exceed the Tier1 threshold by larger factors than 1,1,1-TCA, the maximum concentrations of 1,1,1-TCA are an order of magnitude higher than those for TCE. A comparison of mass contained in the various phases indicates that a large portion (~75% for 1,1,1-TCA and ~60% for TCE) of the contaminant mass is contained in the vapor phase due to high volatility of these compounds and the low water and organic content of the tuff. The breakdown by geologic zone reveals that 80% of the mass for both contaminants is contained within the Tshirege Member of the Bandelier Tuff. A comparison of mass above and below 10 times (10x) the Tier1 screening threshold shows that 1,1,1-TCA mass is almost evenly distributed between these two groups whereas only 5% of the TCE mass is contained by the 1x-10x contaminant plume isoshell. Lastly, Table 3-1 shows that approximately one third of the contaminant mass for both plumes is contained within the 125-ft ROI for the current SVE system configuration. Because the 215-ft SVE wells are completed only into the Qbt1g unit of the Tshirege, the 7% of the total plume mass that is within the ROI but below the Tshirege is not expected to be captured immediately by SVE. However, the reversal of concentration and pressure gradients will likely lead to this VOC mass moving in the direction of the SVE boreholes over time. The eastern SVE ROI intersects approximately 50% more contaminant mass within the Tshirege than the western SVE ROI. However, due to three-dimensional effects, such as asphalt placement, the western SVE unit has historically pulled an initially higher VOC mass from the subsurface than the eastern unit, while at longer times the eastern unit maintains higher concentrations and thus longer-term mass removal.

Table 3-2 presents the results of the uncertainty analysis for the Q4FY14 plume evaluation. The mean and standard deviation of the 36 minimum tension data interpolations for each contaminant were calculated and used to generate mass estimates at different confidence levels assuming a normal distribution. The mass estimate based on the mean was very close to that of the best estimate. The disparity from the best estimate doubles with each 15% increase in confidence level to an outer bound of approximately 30% difference from the best estimate at the 95% confidence level. The mean and 95% confidence plumes can be viewed and printed by toggling on the pdf layers that are turned off by default. This uncertainty analysis includes only interpolation impacts and does not include uncertainty due to variability in sampling conditions (e.g. soil gas humidity and operator inconsistency) discussed in the introduction.

3.2 Comparison with FY11

Plume interpretations for FY11 are presented in Figures 3-3 through 3-10. They are grouped by contaminant and sorted chronologically. The overall shape and lateral extent of both plumes is relatively consistent through time; however, source concentrations and the vertical extent of both plumes vary. Source concentrations of both contaminants were consistently higher during FY11 than in Q4FY14 but the inner plume region (e.g. the 10x contour for 1,1,1-TCA and the 50x contour for TCE) was generally shallower than that of Q4FY14. The Q1 and Q4FY11 distributions were similar to each other and exhibited higher concentrations than Q2 and Q3FY11. The 10x contour for 1,1,1-TCA was constrained to the Tshirege member of the Bandelier tuff during most of FY11 (penetrating the Qct interval only during Q1FY11, whereas it extended nearly to the base of the deeper Otowi member of the Bandelier Tuff (Qbof) during Q4FY14. The 50x contour for TCE penetrated Qbof during Q1 and Q2FY11 but penetrated the underlying Tb4 during Q4FY14. To summarize, Q4FY14 exhibits the lowest source concentrations but the highest deep (Qct and Qbof) concentrations of the five quarters. The reduced source concentrations during the middle of FY11 indicate that there may be sampling variability superimposed on the potential long-term trend of decreasing source concentrations through time. The elevated deep concentrations during Q4FY14 may be an indication of a new long-term trend. These trends will be further analyzed as more data become available.

The trends observed in Figures 3-1 through 3-10 are reflected in the interpolated mass estimates presented in Table 3-3. This table uses the same structure as Table 3-1 to show differences in the total mass (all three contaminant phases) among the various quarters. It shows that Q3FY11 had the lowest plume mass of the five quarters for both contaminants. Q1 and Q4FY11 mass estimates were closer to those of Q4FY14 but the distribution of mass was different. They each contained more 1,1,1-TCA mass than Q4FY14 within the Tshirege but much lower 1,1,1-TCA mass below the Tshirege. The lower portion of Table 3-3 indicates that the overall variation in plume mass among all quarters was approximately 35% for both 1,1,1-TCA and TCE. Contaminant mass varied by 70% below the Tshirege but this region contributes only 20% of the overall mass so overall fluctuations are more similar to the fluctuations within the Tshirege. The right-hand side of Table 3-3 provides the percentage of overall mass contained by the SVE ROI for each quarter. These numbers show that although the overall plume mass fluctuates considerably through time, the proportion of mass within the ROI remains steady at approximately 30% for 1,1,1-TCA and 33% for TCE.

Quarterly plume monitoring within these ROIs, annual monitoring over the broader plume, and periodic extraction gas monitoring are all being completed as part of the Interim Measures Work Plan (LANL 2014, 261843) to quantify the mass removed by the interim SVE system. The relative consistency of the proportion of overall plume mass within the ROIs prior to the commencement of SVE will likely allow trends in the data collected during SVE operation to be distinguished from the natural temporal variability.

Figures 3-11 and 3-12 were prepared to help visualize why the overall mass of contaminants was highest in Q4FY14 despite source concentrations of both contaminants that were among the lowest during this quarter. Figure 3-11 shows that the variability in mass estimates is largest within the >10x portion within the Tshirege for both contaminants. This interval comprises almost 50% of the 1,1,1-TCA mass and 85% of the TCE mass. Figure 3-12 breaks the mass up by concentration isoshells to better identify where the majority of mass is estimated to reside within the Tshirege unit. This figure shows that isoshells ≥20x contribute very little to the 1,1,1-TCA mass but contribute most of the TCE mass. For 1,1,1-TCA, the 10x isoshell (medium blue contour line and light blue filled contour on the 1,1,1-TCA plume figures) contributes the most to overall 1,1,1-TCA plume mass. For TCE, the 50x and 100x isoshells (red contour line and yellow/orange filled contours on the TCE plume figures) contribute the most to the overall TCE plume mass. These isoshells are the ones most affected by the slightly elevated concentrations in the deepest ports of borehole 54-27642. Because these ports are bounded better to the southeast than they are to the northwest, the model is very sensitive to concentration variations in these two ports. In essence, the relatively small concentration increase at these two deep ports had a larger impact on the overall plume mass than more significant shallow concentration reductions because the ports in source areas (e.g. 54-02089 and 54-24238) were better bounded by other data.

Figures 3-13 and 3-14 provide a comparison of the Q4FY14 results to each of the FY11 quarters using scatterplots with a 1:1 line superimposed. Both figures show that the Q4FY14 concentrations are generally lower than each of the FY11 quarters, especially at the higher concentrations. However there are several outliers for which the concentrations are much higher in Q4FY14 than in any of the FY11 quarters. The most notable of these outliers are the 275’ and 338’ ports of borehole 54-27642, which are the primary drivers for the relatively deeper contamination depicted in Figures 3-1 and 3-2. These outliers are of particular interest and will be further analyzed for indication of a long-term trend as additional data become available during the interim measures monitoring.

Figures 3-15 through 3-26 provide time-series vapor-phase concentrations from FY09 to the present (Q4FY14) for all 85 routinely sampled ports. On each figure, multiple ports are plotted on a single page to facilitate comparisons among ports at similar depths (grouped by intervals of 20-ft) and to visualize trends going down each borehole. The figures are grouped by compound (parent compounds versus daughter products), scaling on the y axis (arithmetic versus log), and plume region (source areas, inner plume region, and plume margins). These groupings facilitate comparison of trends among the different compounds in similar plume regions using different scales to highlight different aspects of the data.

Figure 3-15 uses an arithmetic scale to present 1,1,1-TCA and TCE trends within the source areas. This figure shows generally decreasing concentrations of parent compounds at most ports with some temporal variability superimposed. The aforementioned outliers from Figures 3-13 and 3-14 (deepest ports at 54-27642) are plotted in the bottom right and show an increase of both contaminants. Several other ports (e.g. all of the 54-24243 ports and the 40-ft port at boring 54-24240) show a less pronounced increase of at least one parent compound but only between Q4FY11 and Q4FY14. The inner plume ports depicted on Figure 3-16 also show generally decreasing concentrations of parent compounds through time. The outer plume concentrations, which are only discernible on log scale (Figure 3-20), generally present more stable concentrations through time than the source area and inner plume ports. The log scale plot of daughter products in the source areas (Figure 3-24) show declining trends at several ports but there appear to be fewer ports that show declining trends of daughter products than show declining trends of parent compounds. The log scale plots of inner plume (Figure 3-25) and plume margin (Figure 3-26) daughter products also reveal stable or increasing concentrations at several ports that showed decreasing concentrations of parent compounds.

The trends exhibited in Figures 3-15 through 3-26 are complicated by temporal variability. For example, the increasing trend at the 260-ft port of 54-27642 (bottom right of Figure 3-18) is interrupted by a sharp decrease during FY11. This decrease, although generally not as pronounced as in 54-27642 and observed predominantly during Q2 and Q3FY11, was observed in at least half of the ports and is responsible for the lower mass estimates for Q2 and Q3FY11 compared to the other three quarters. The log-scale figures show that the FY11 decrease affects both parent and daughter compounds in all portions of the plume, regardless of whether there was an increasing or decreasing trend. This rapid change in concentrations is not expected from the physical conceptual model of the site and may be related to sampling variability factors discussed in the introduction.

Although the concentrations of parent compounds have generally declined at many ports in the network, concentrations have increased at the two deepest ports (275' and 338') in 54-27642. The interpolated plume masses are especially sensitive to these two ports because of a relative lack of deep data immediately northwest of these ports. Elevated Q4FY14 TCE concentrations at the two other ports completed in the Qct interval (boreholes 54-27641 and 54-27643) suggest that the increase in 54-27642 is not an anomaly.

4 CONCLUSIONS

Analysis of the most recent five quarters of MDA L data has revealed several important findings. The Q4FY14 round of data, which is to be used as the baseline for evaluating the effectiveness of the SVE interim measure, exhibits some of the lowest 1,1,1-TCA and TCE concentrations near the source shafts observed at many ports. However, Q4FY14 has also yielded the highest integrated plume mass of both contaminants from among the last five quarters. The reason for this apparent discrepancy is the relative contribution of different plume regions to the overall mass. For 1,1,1-TCA, the isoshells ≤10 times the Tier1 threshold contribute much more mass to the total than isoshells ≥20x. For TCE, the 50x and 100x isoshells contribute the most mass to the total. In other words, pronounced decreases in source area mass can be offset by a more subtle mass increase estimated for the rest of the plume. Concentrations in the two deepest ports (275' and 338') have created precisely this condition, resulting in an increase in interpolated far-field plume mass from FY11 to Q4FY14. The seven ports in borehole 54-27642 will be sampled quarterly during the SVE interim measure to supply additional data for further evaluation of contaminant concentrations within this borehole.

Despite the quarterly fluctuations in overall interpolated plume mass, the proportion contained within the predicted footprint of the SVE ROI is relatively steady. This means that a significant decline in the ratio of the mass within the ROI to the total plume mass will clearly be attributable to VOC mass removal by the SVE system.

REFERENCES

ASTM (American Society for Testing and Materials), 2006. "Standard Guide for Soil Gas Monitoring in the Vadose Zone," D 5314 – 92 (Reapproved 2006), West Conshohocken, Pennsylvania. (ASTM 2006, 110404 . http://www.astm.org/Standards/D5314.htm)

Dynamic Graphics, Inc. October, 2014. earthVision Version 9.0. Reference Manual.

LANL (Los Alamos National Laboratory), March 2009. "Numerical Analysis of the Soil-Vapor Extraction Test at Material Disposal Area G, Technical Area 54," Los Alamos National Laboratory document LA-UR-09-0995, Los Alamos, New Mexico. (LANL 2009, 105413)

LANL (Los Alamos National Laboratory), September 2011. "Corrective Measures Evaluation report for Material Disposal Area L, Solid Waste Management Unit 54-006, at Technical Area 54, Revision 2" Los Alamos National Laboratory document LA-UR-11-4798, Los Alamos, New Mexico. (LANL 2011, 205756)

LANL (Los Alamos National Laboratory), September 2014. "Interim Measures Work Plan for Soil-Vapor Extraction of Volatile Organic Compounds from Material Disposal Area L, Technical Area 54, Revision 1" Los Alamos National Laboratory document LA-UR-14-26472, Los Alamos, New Mexico. (LANL 2014, 261843)

NMED (New Mexico Environment Department), August 2009. "Technical Background Document for Development of Soil Screening Levels, Revision 5.0," New Mexico Environment Department, Hazardous Waste Bureau and Ground Water Quality Bureau Voluntary Remediation Program, Santa Fe, New Mexico. (NMED 2009, 106420)

Springer, E.P., 2005. "Statistical Exploration of Matrix Hydrologic Properties for the Bandelier Tuff, Los Alamos, New Mexico," *Vadose Zone Journal,* Vol. 4, pp. 505–521. (Springer 2005, 098534)

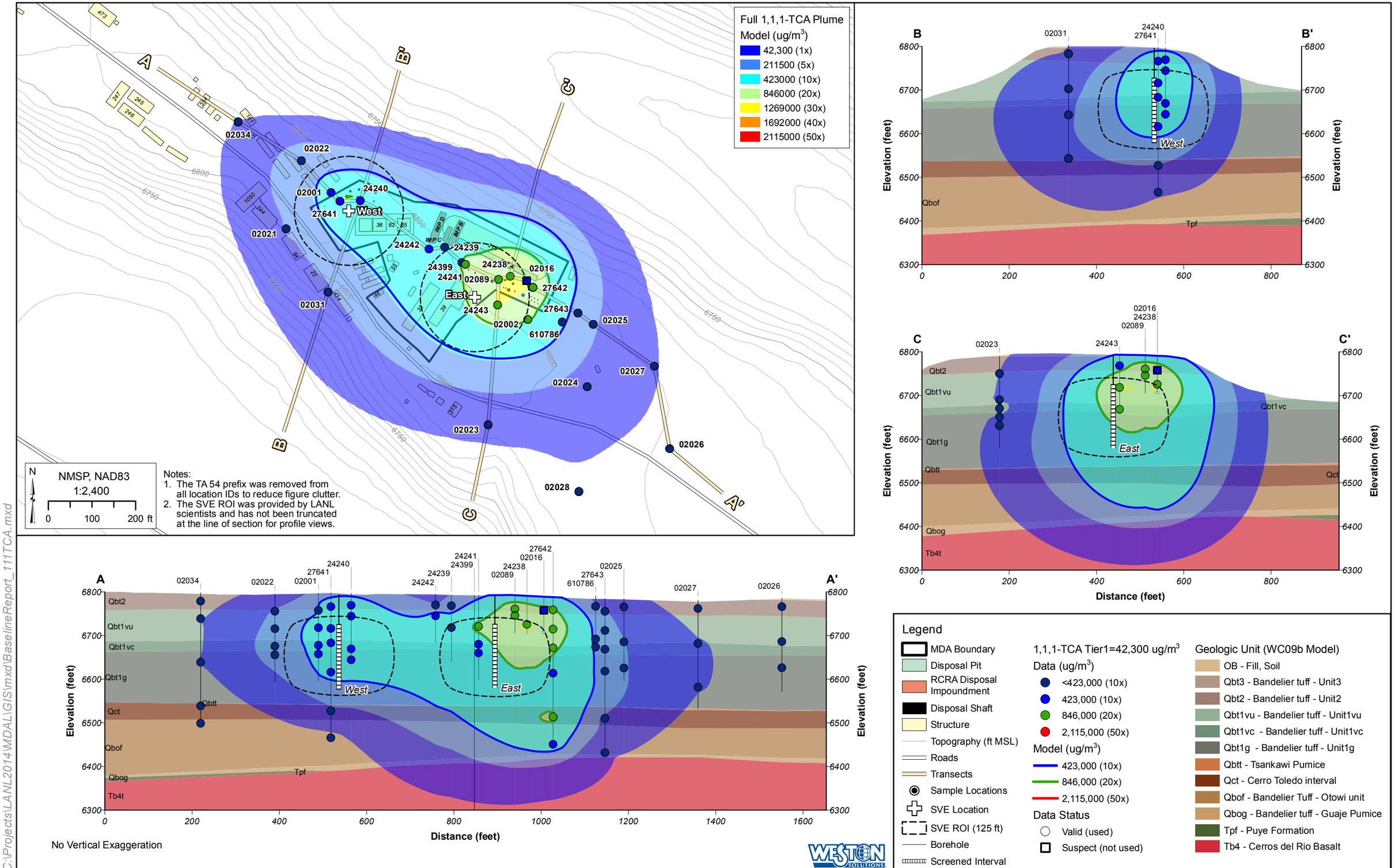

Figure 3-1 MDA L Subsurface 1,1,1-TCA vapor distribution for Q4FY14

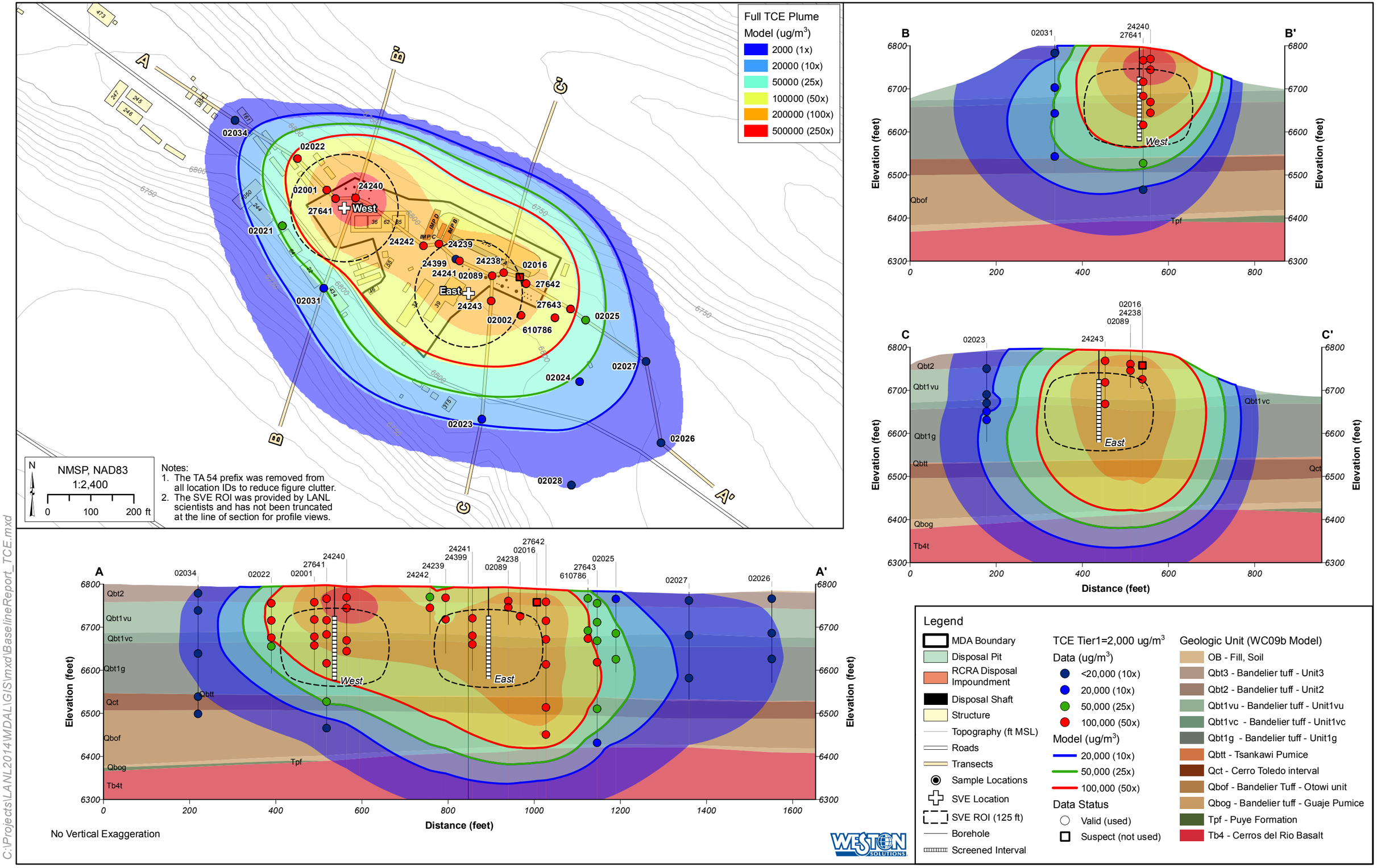

Figure 3-2 MDA L Subsurface TCE vapor distribution for Q4FY14

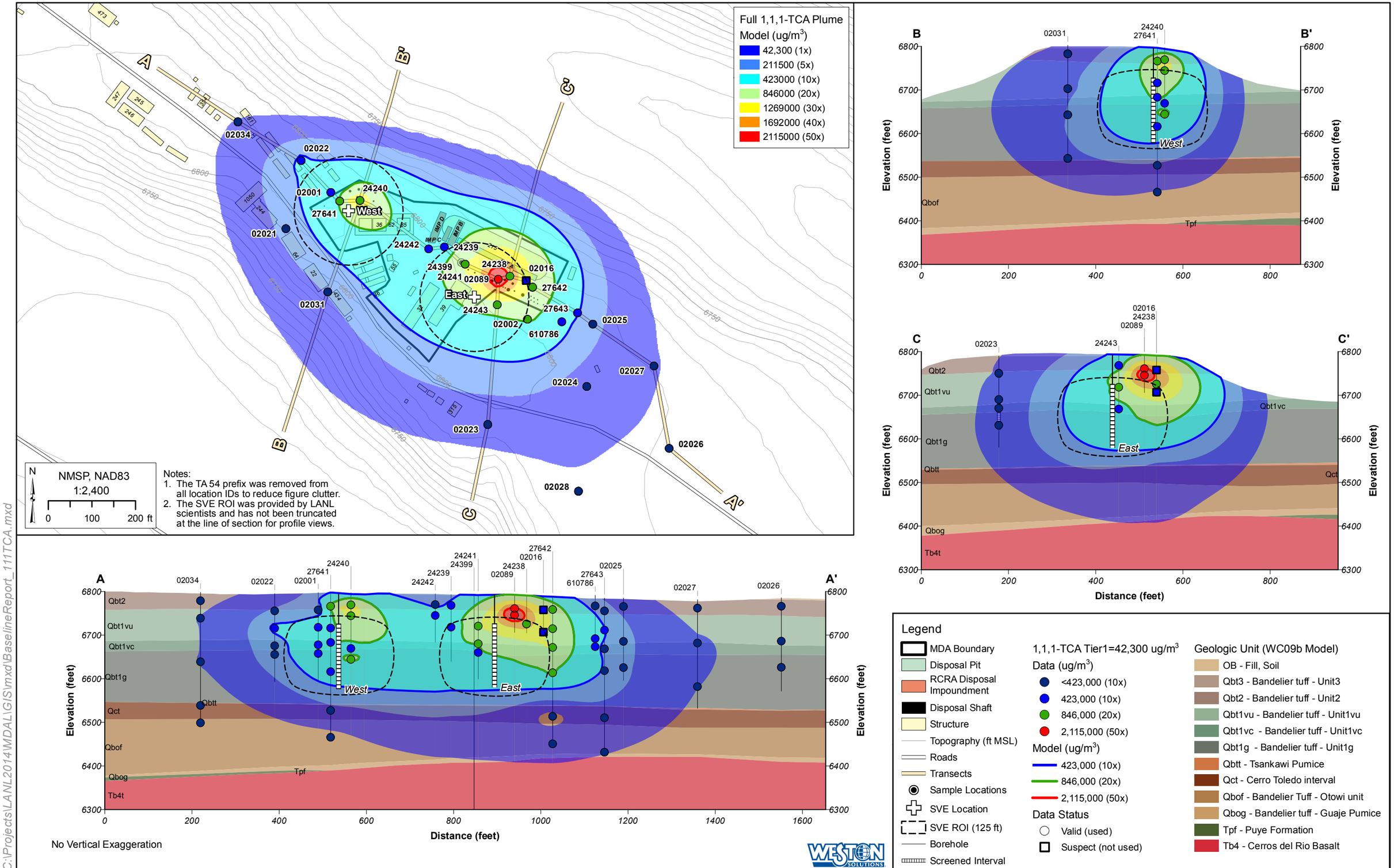

Figure 3-3 MDA L Subsurface 1,1,1-TCA vapor distribution for Q4FY11

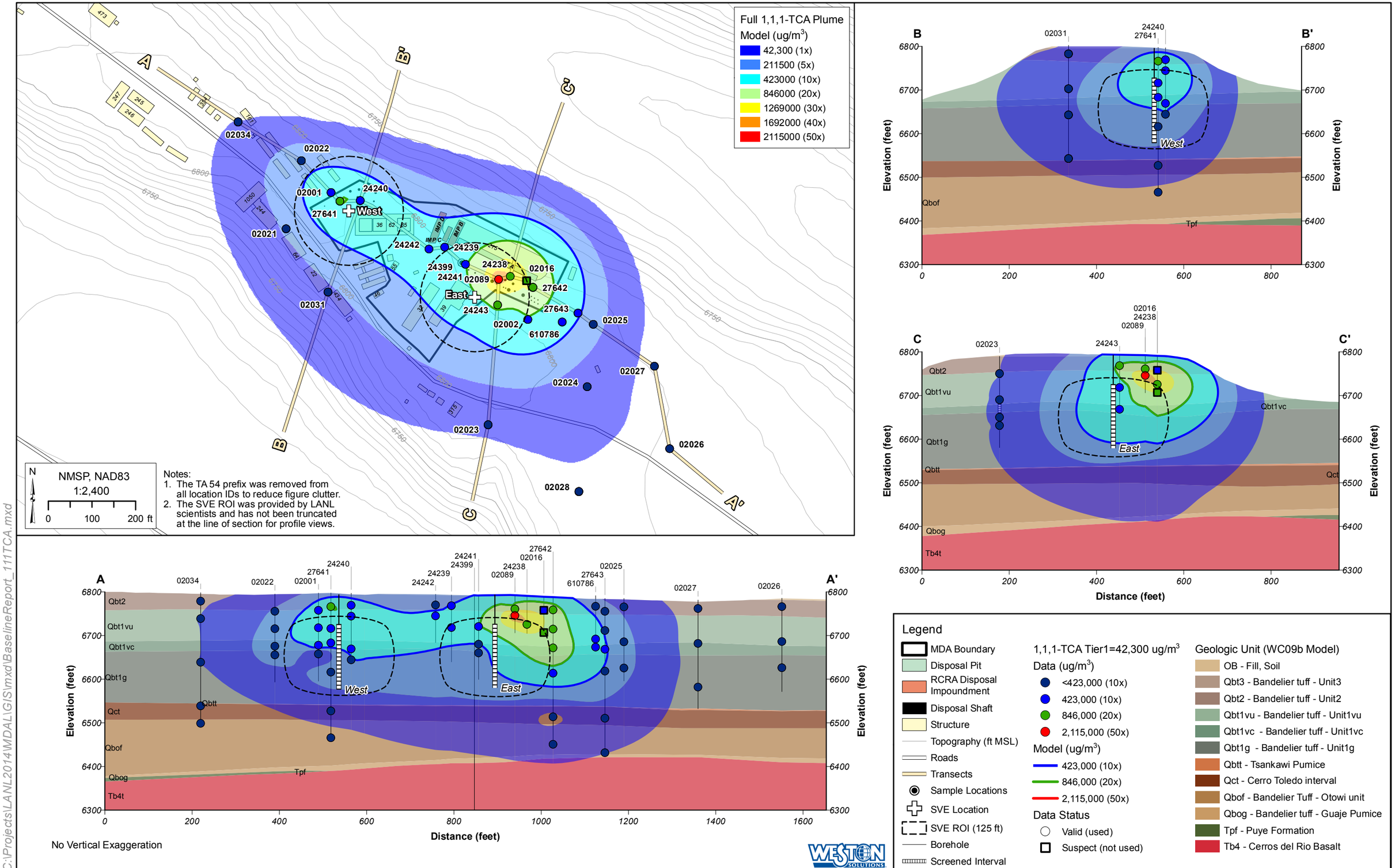

Figure 3-4 MDA L Subsurface 1,1,1-TCA vapor distribution for Q3FY11

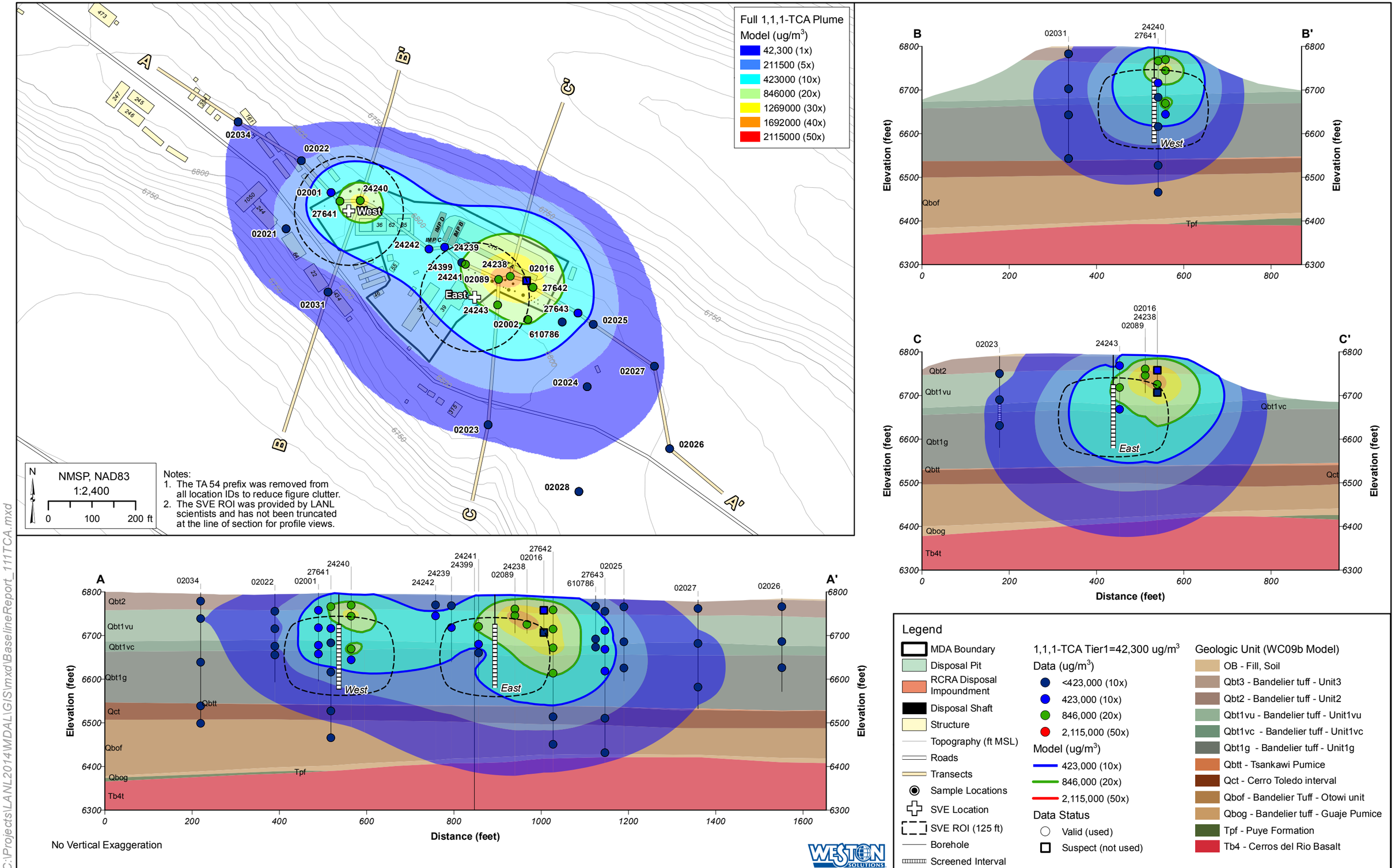

C:\Projects\LANL2014\MDAL\GIS\mxd\BaselineReport_111TCA.mxd

Figure 3-5 MDA L Subsurface 1,1,1-TCA vapor distribution for Q2FY11

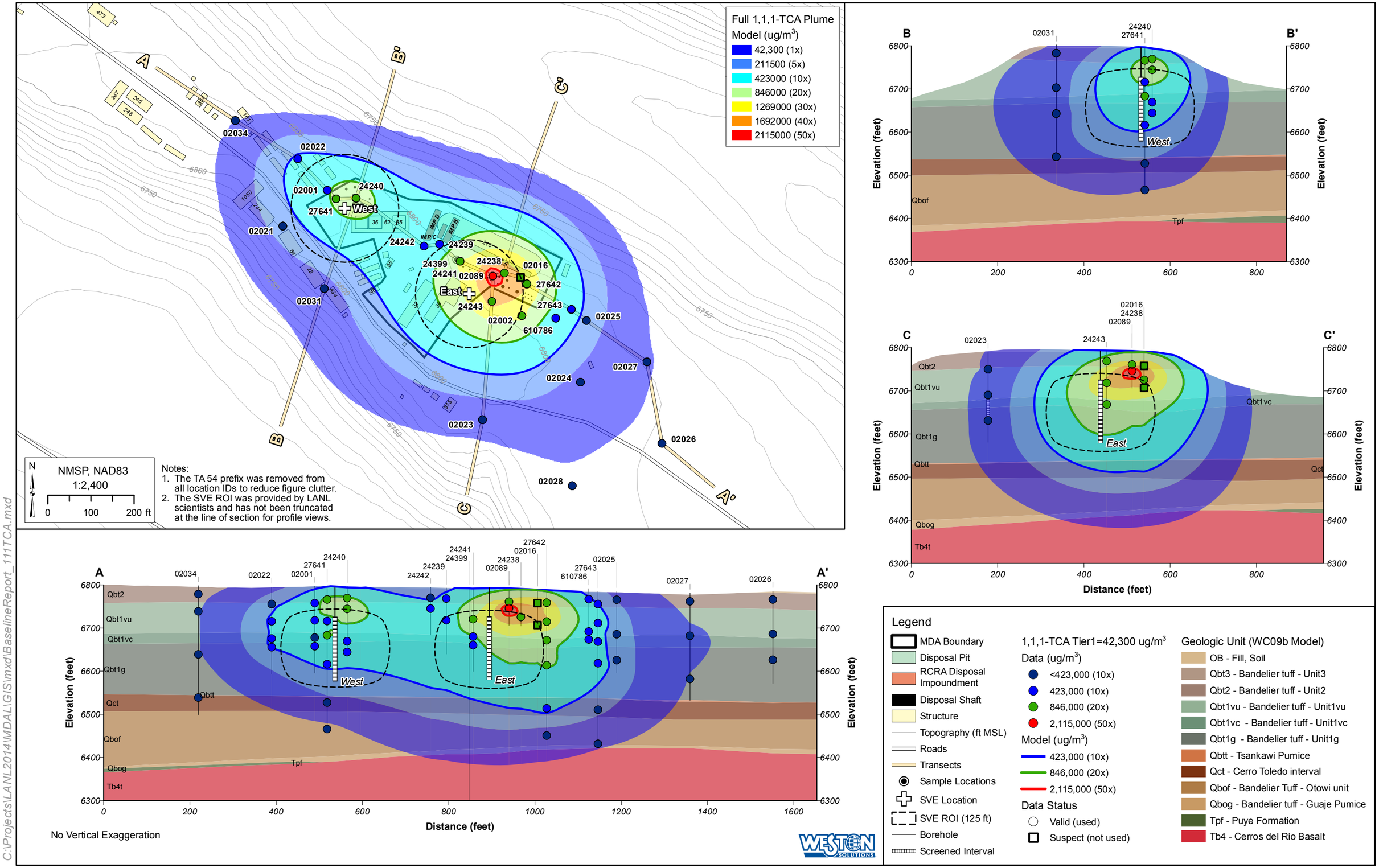

Figure 3-6 MDA L Subsurface 1,1,1-TCA vapor distribution for Q1FY11

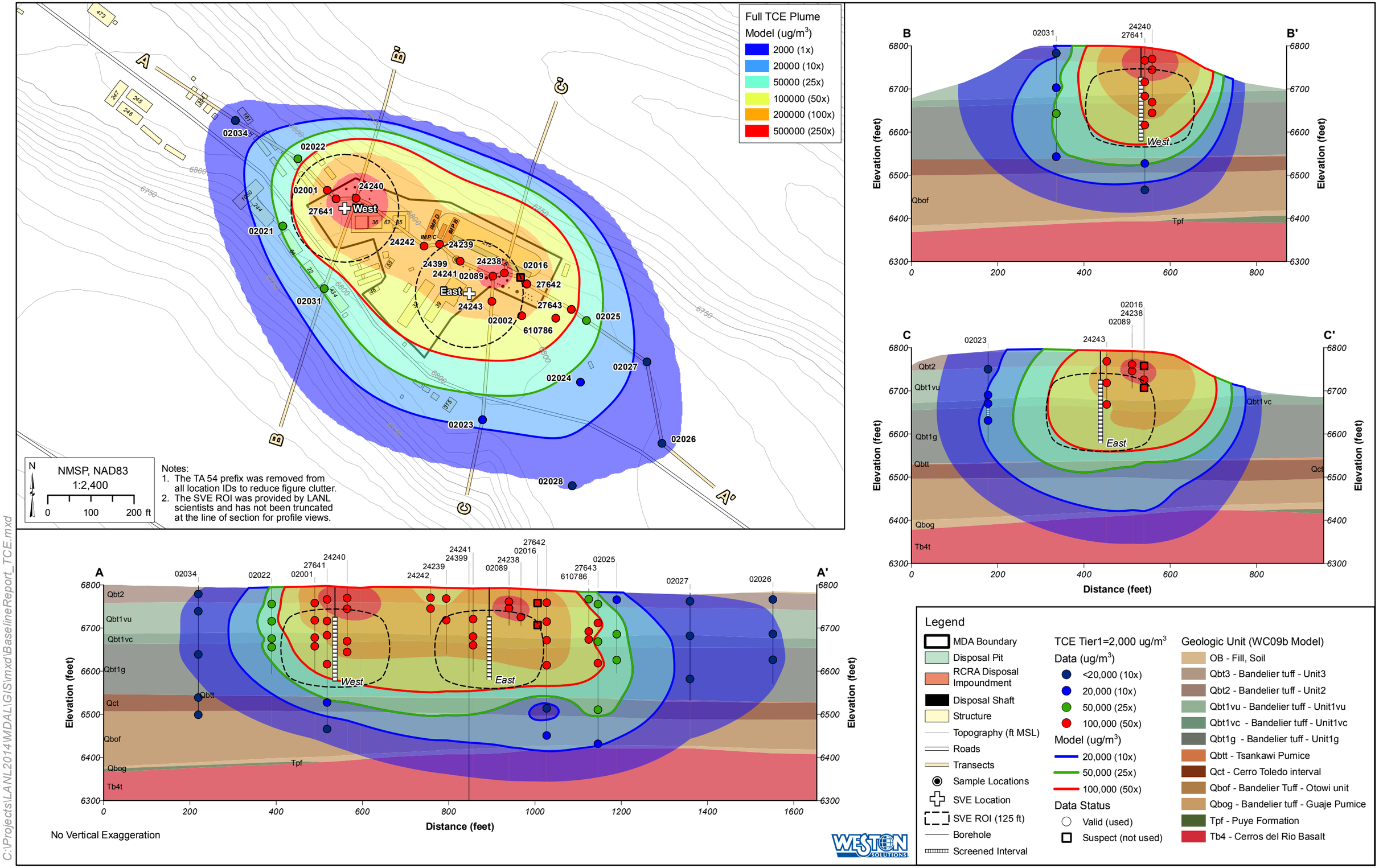

Figure 3-7 MDA L Subsurface TCE vapor distribution for Q4FY11

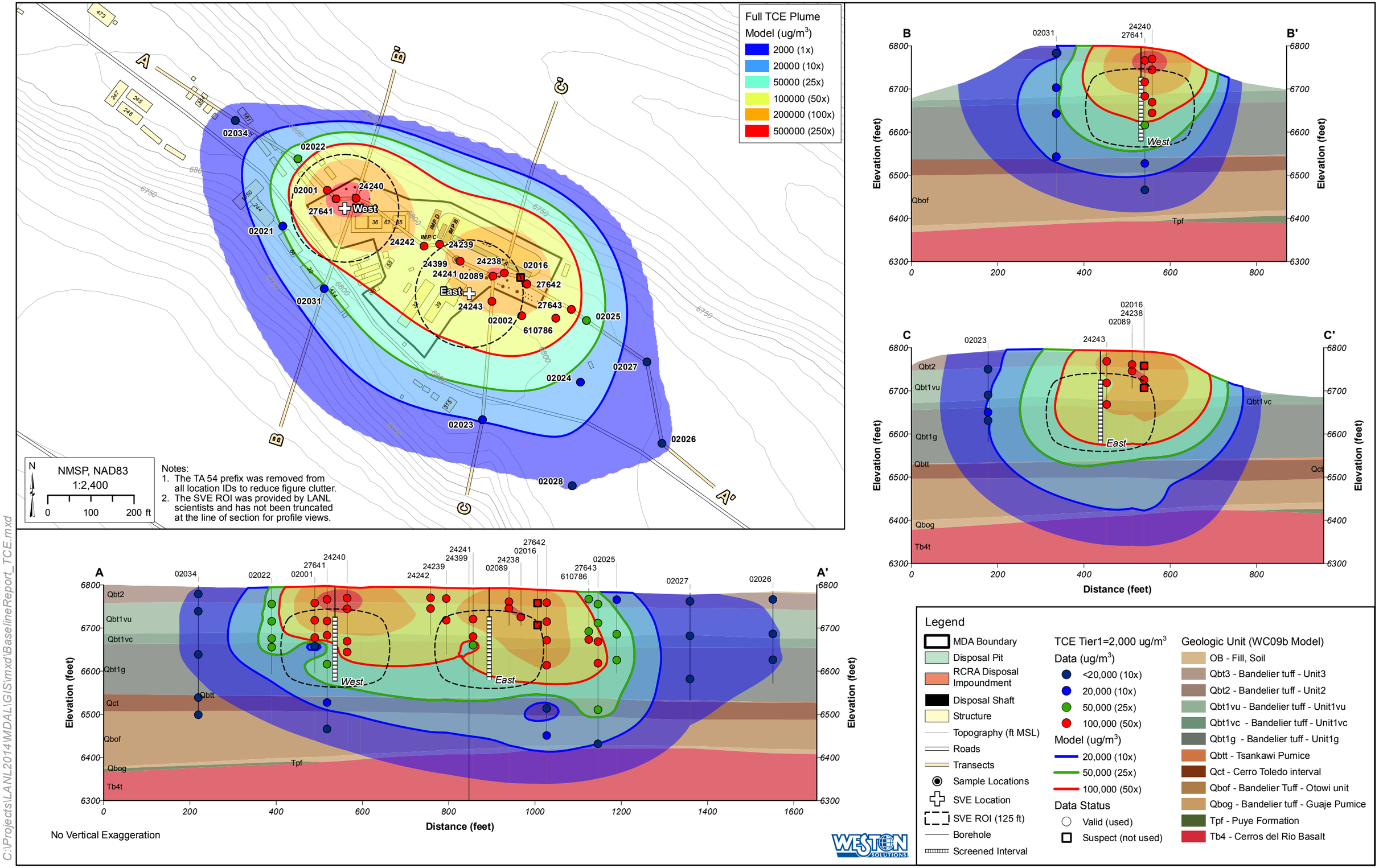

Figure 3-8 MDA L Subsurface TCE vapor distribution for Q3FY11

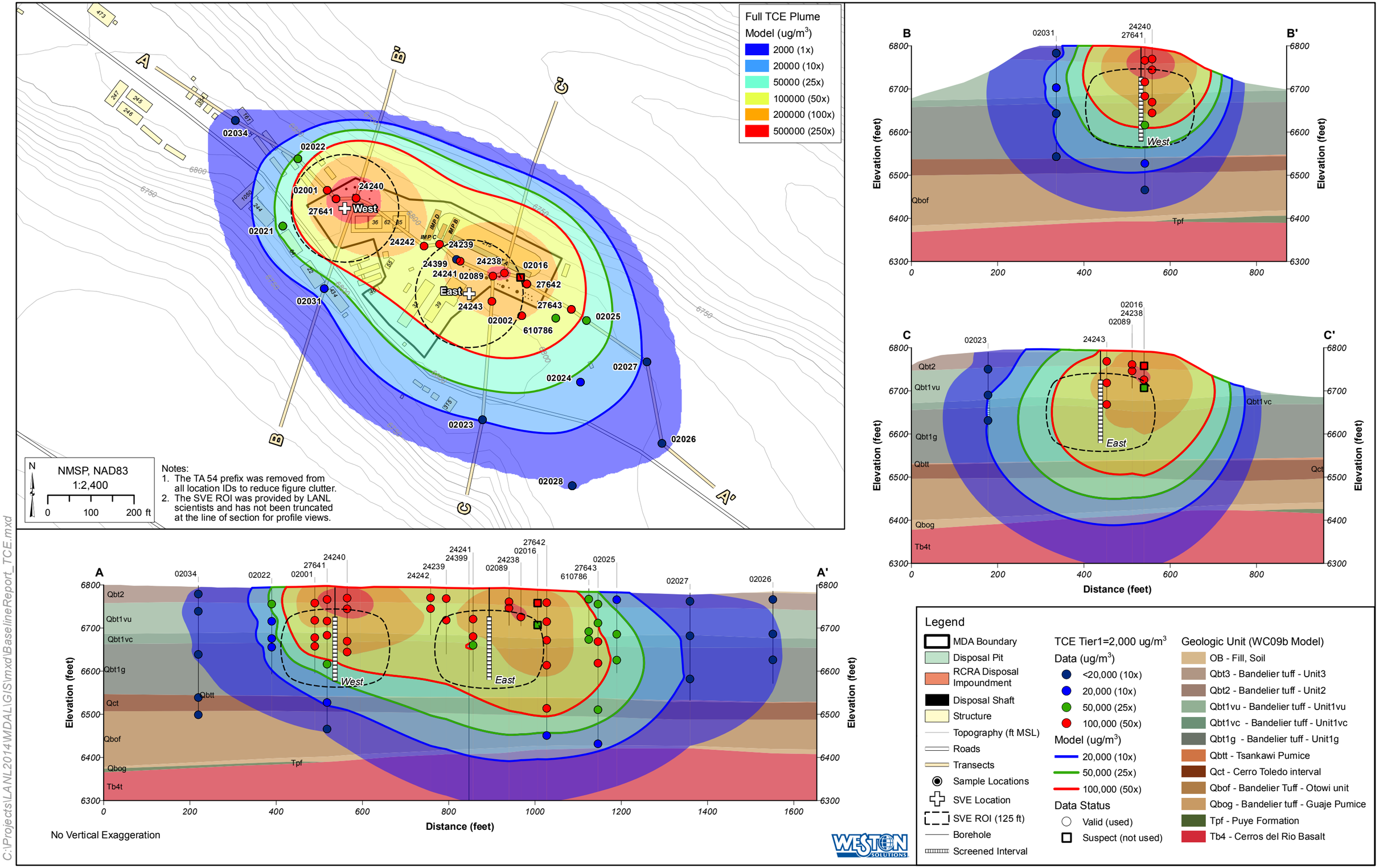

Figure 3-9 MDA L Subsurface TCE vapor distribution for Q2FY11

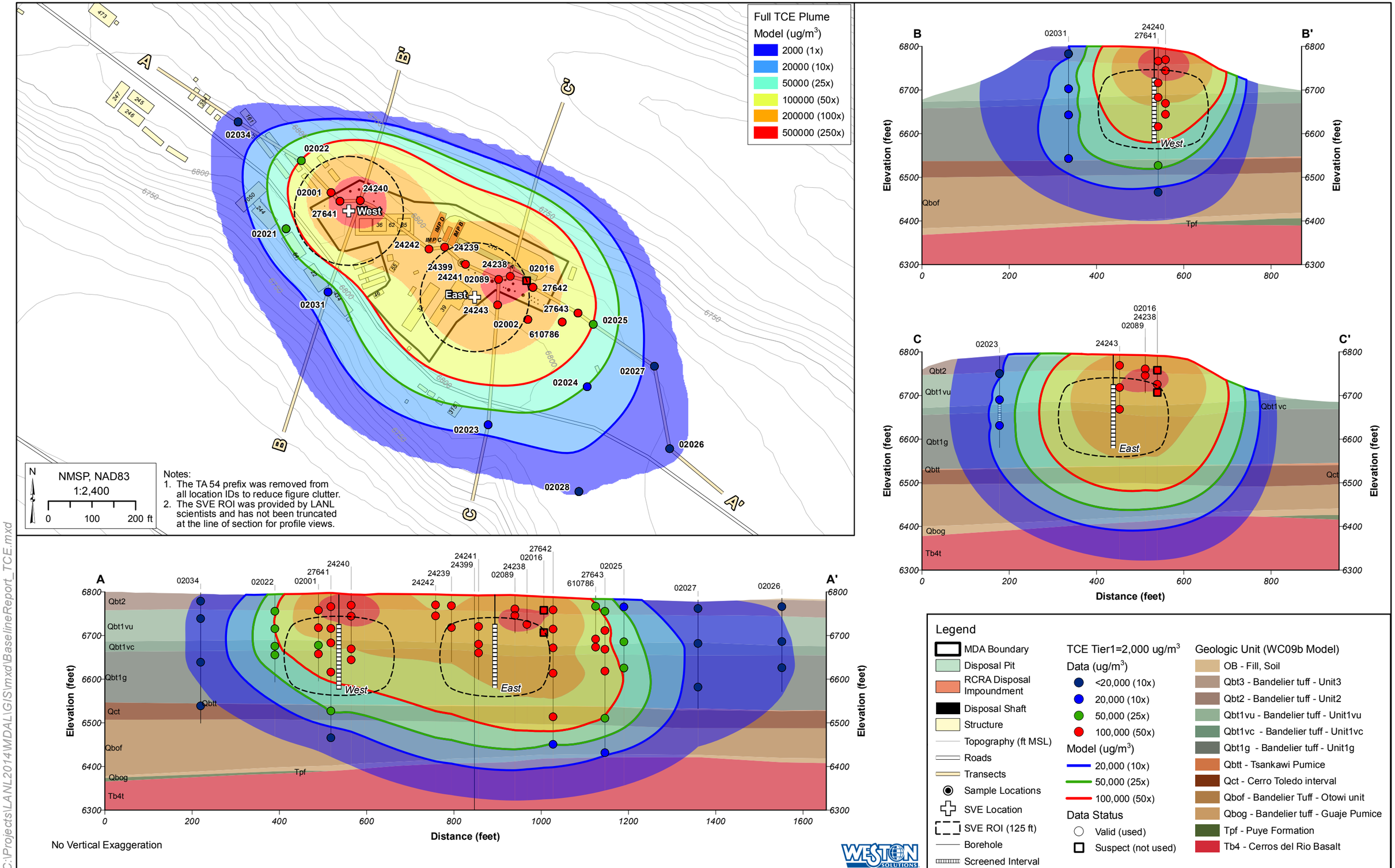

Figure 3-10 MDA L Subsurface TCE vapor distribution for Q1FY11

Figure 3-11
Comparison of Mass Distribution by Quarter

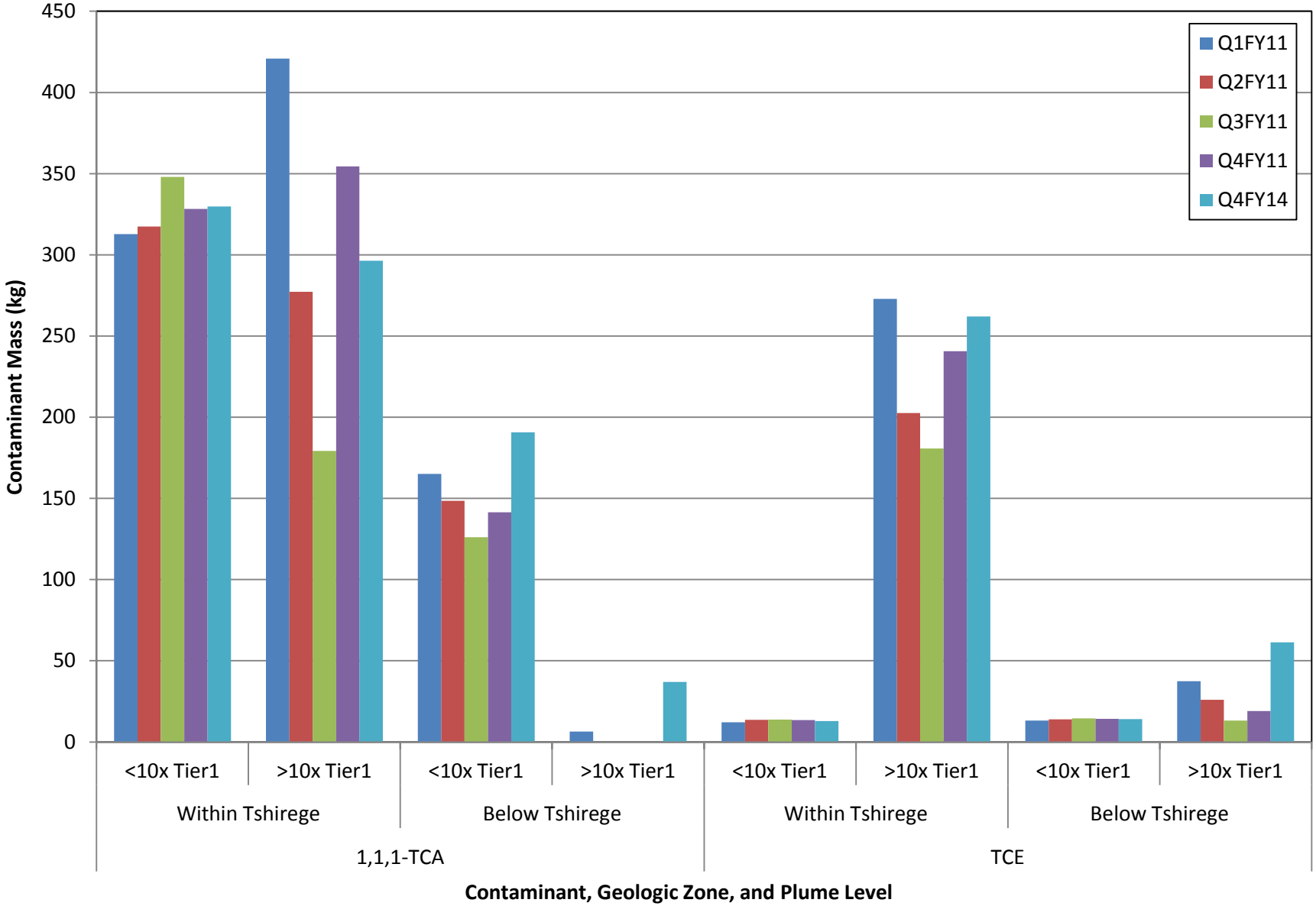

Figure 3-12
Comparison of Mass Distribution by Isoshell and Quarter Within the Tshirege

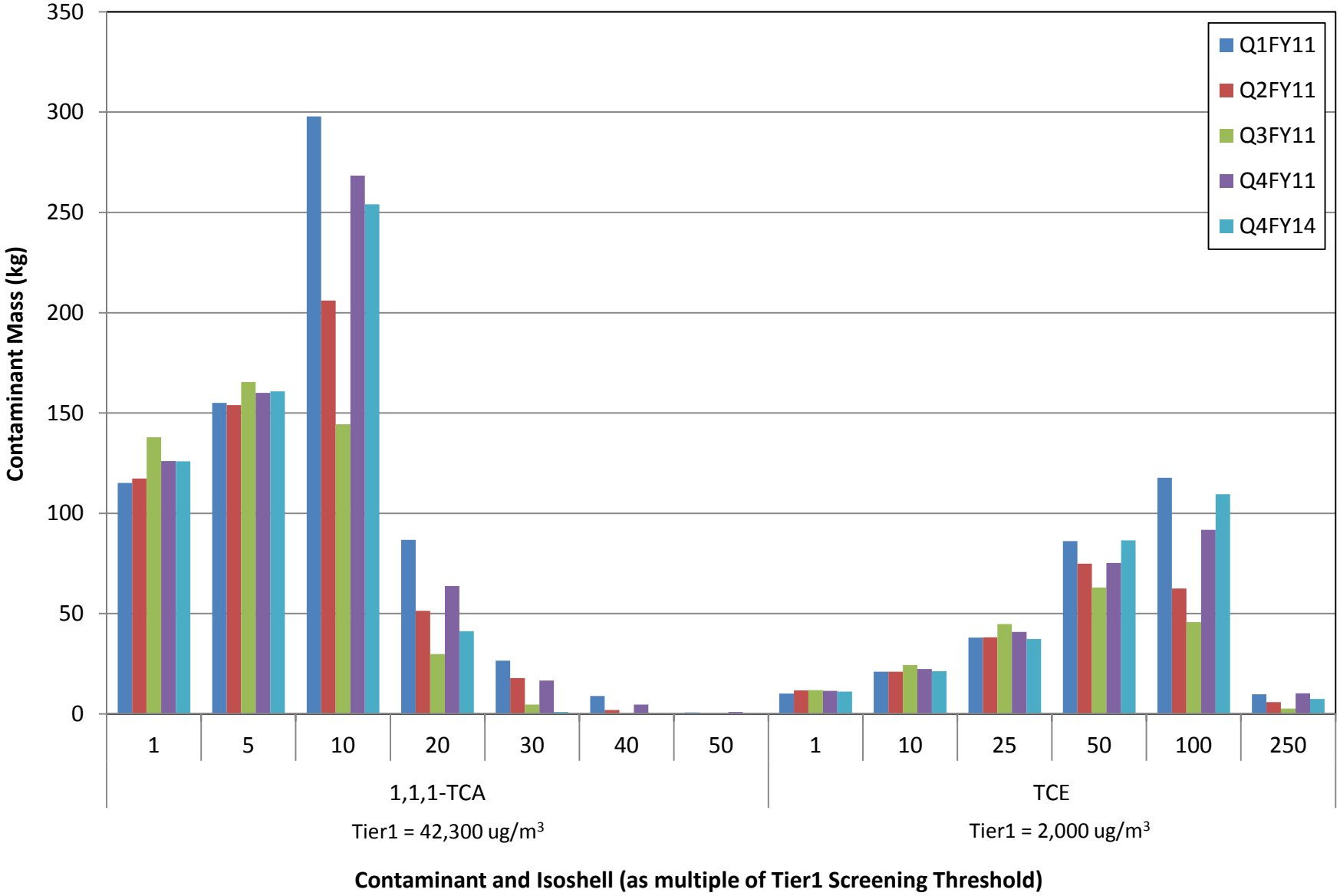

Figure 3−13
Comparison of Q4FY14 1,1,1−TCA Results With FY11

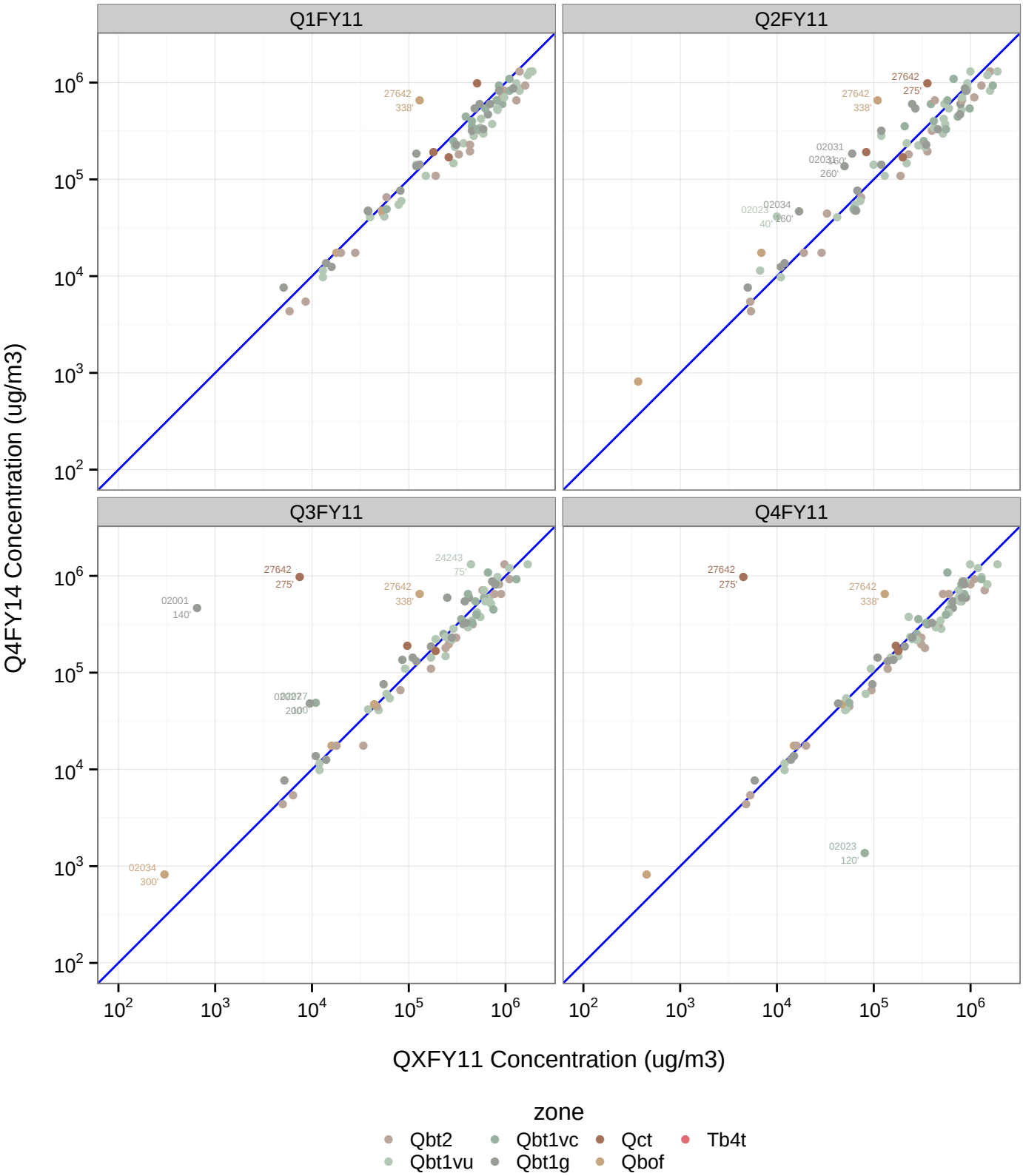

Figure 3−14
Comparison of Q4FY14 TCE Results With FY11

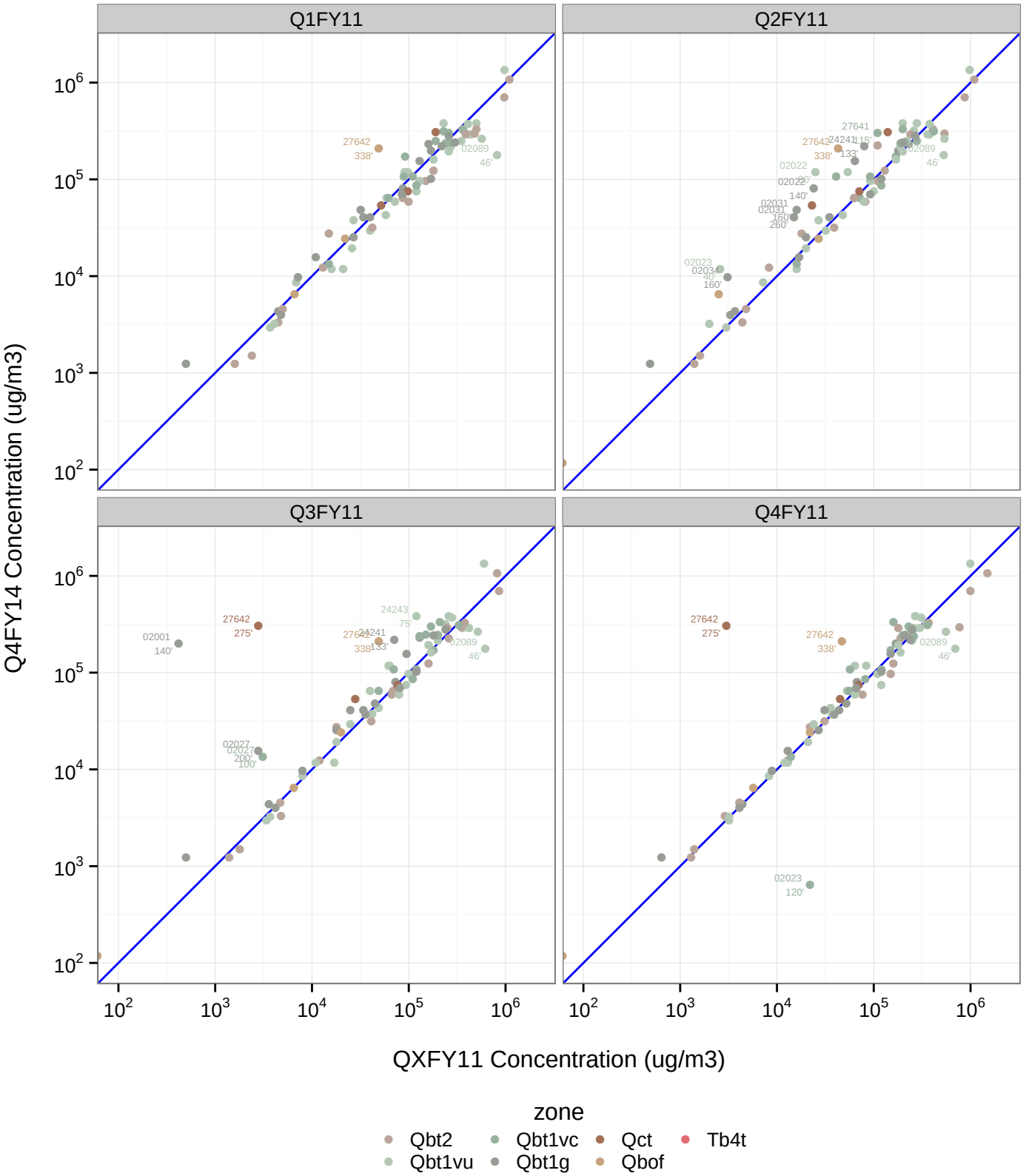

Figure 3−15

Recent Time History of VOC Parent Compounds Within the Source Areas

Port Depth (feet bgs) and year

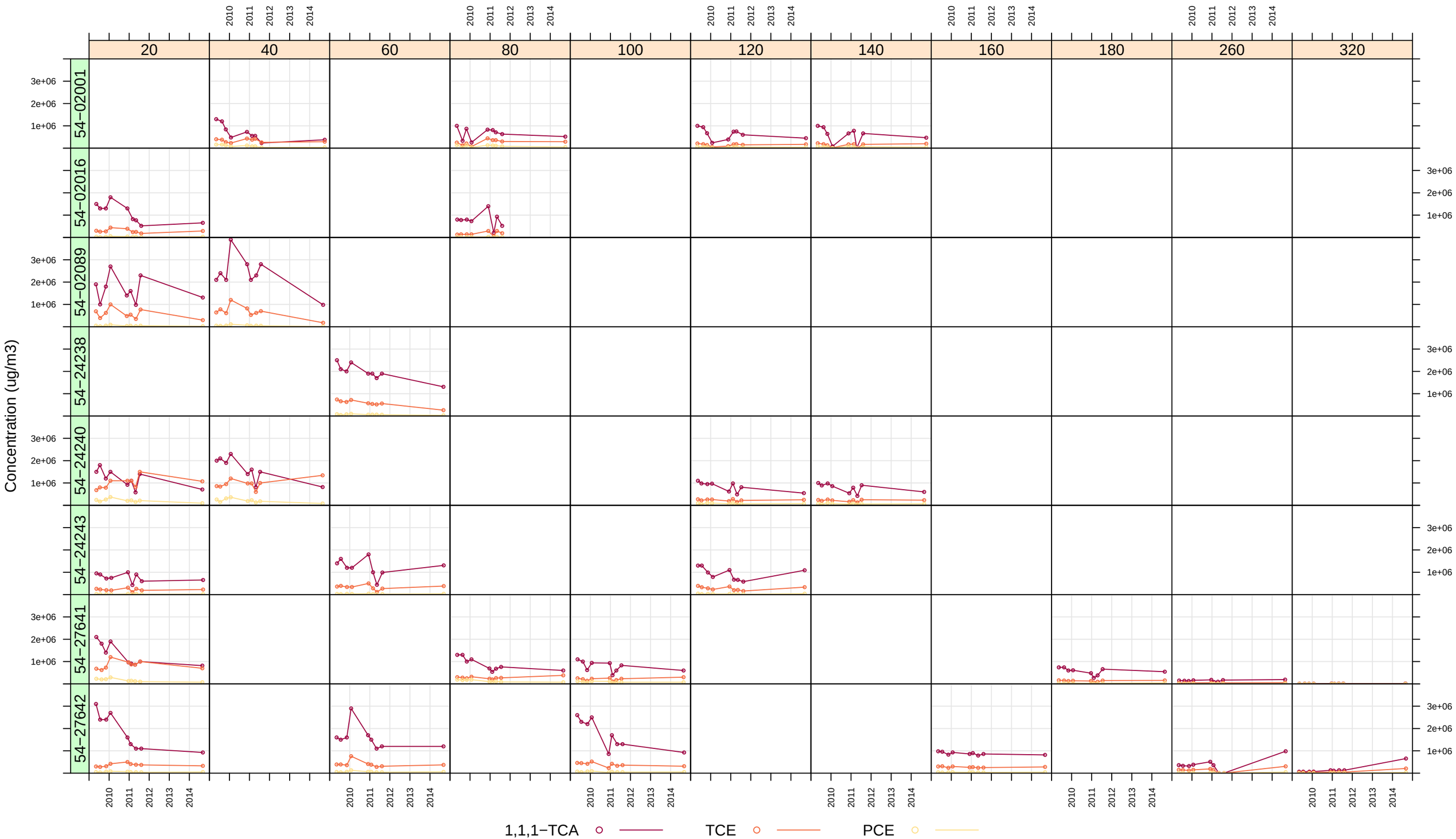

Figure 3−16

Recent Time History of VOC Parent Compounds Within the Inner Plume

Port Depth (feet bgs) and year

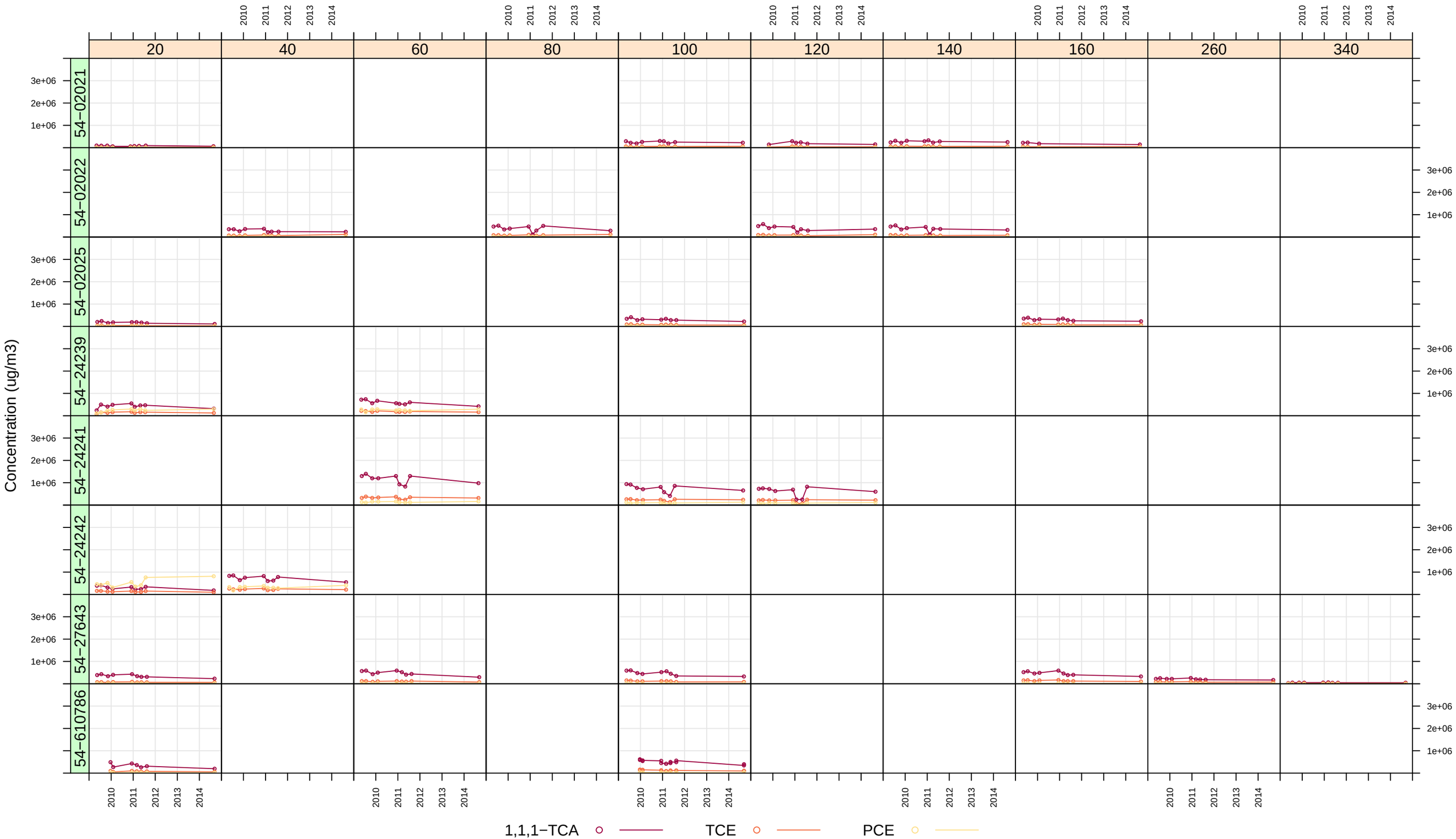

Figure 3−17

Recent Time History of VOC Parent Compounds at the Plume Margins

Port Depth (feet bgs) and year

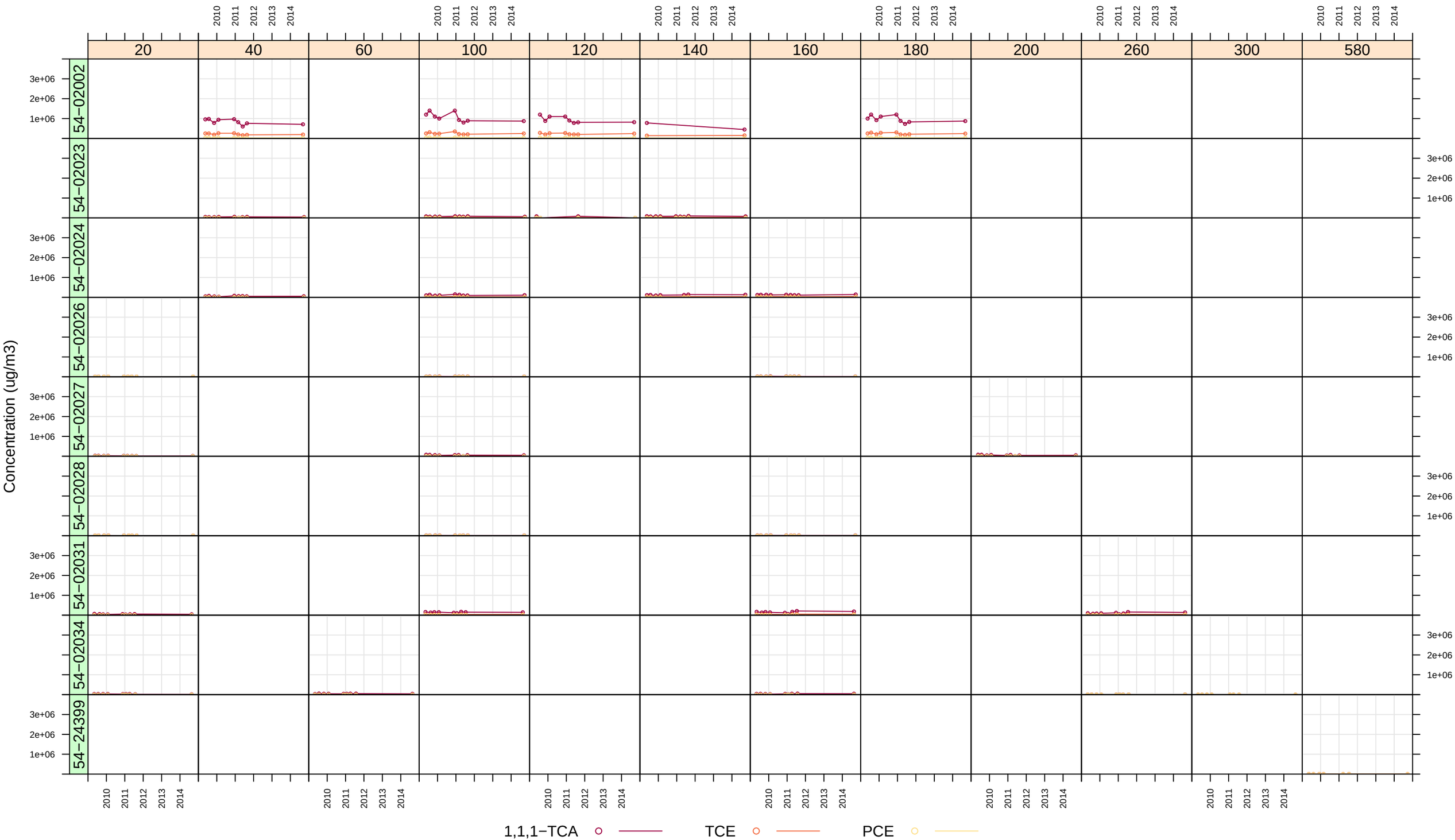

Figure 3−18

Recent Time History of VOC Parent Compounds Within the Source Areas (log scale)

Port Depth (feet bgs) and Year

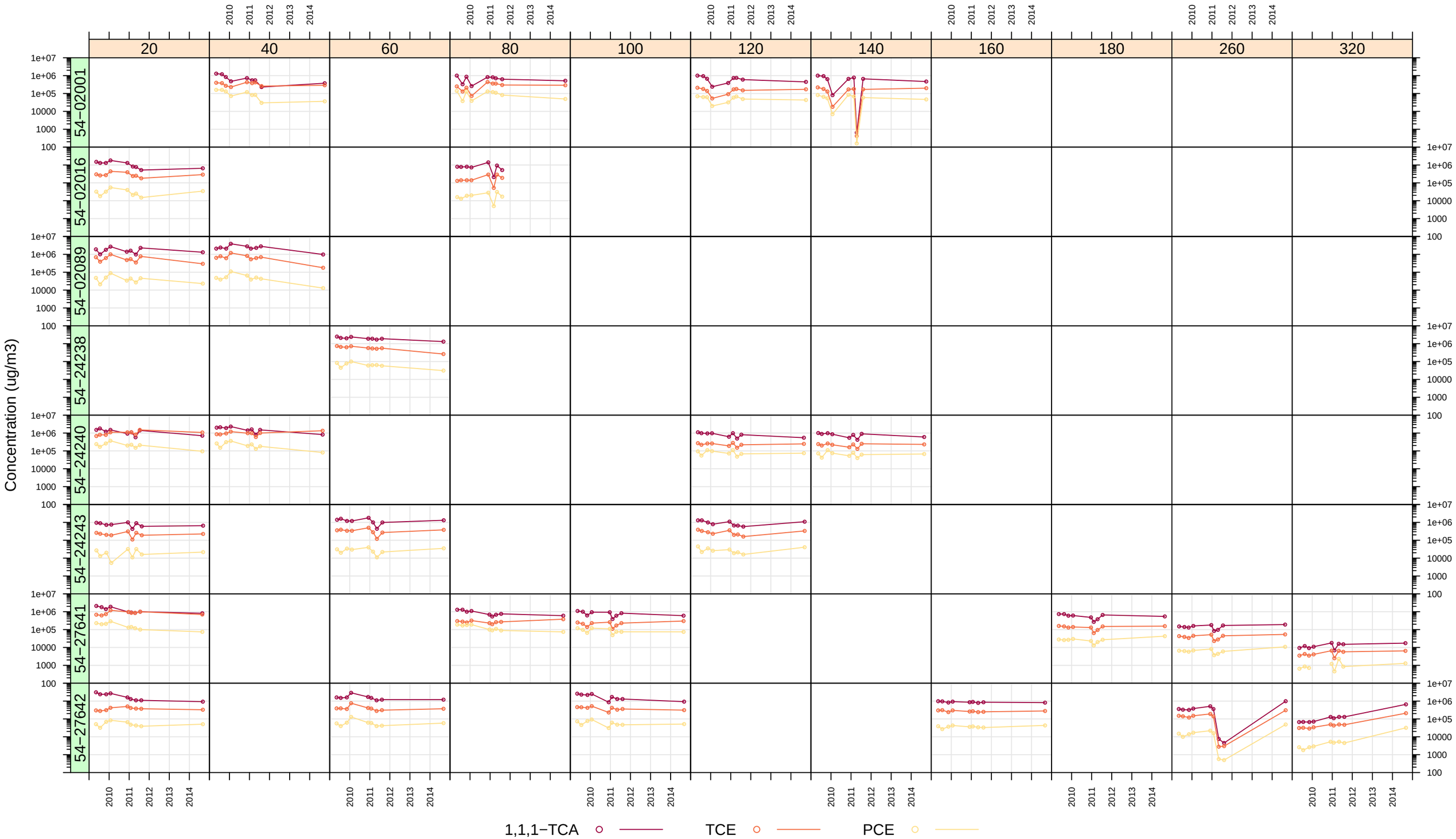

Figure 3−19

Recent Time History of VOC Parent Compounds Within the Inner Plume (log scale)

Port Depth (feet bgs) and Year

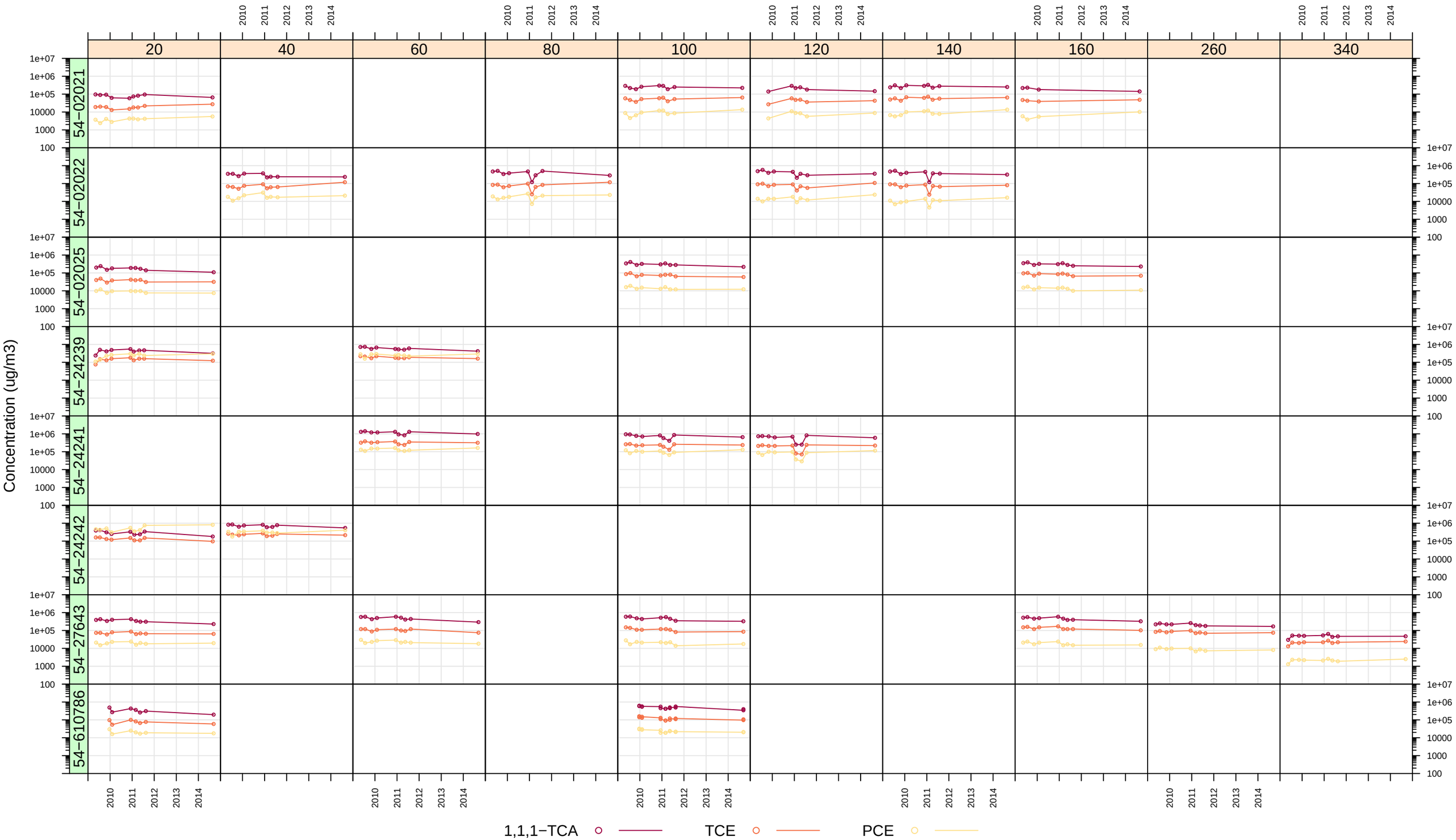

Figure 3−20

Recent Time History of VOC Parent Compounds at the Plume Margins (log scale)

Port Depth (feet bgs) and Year

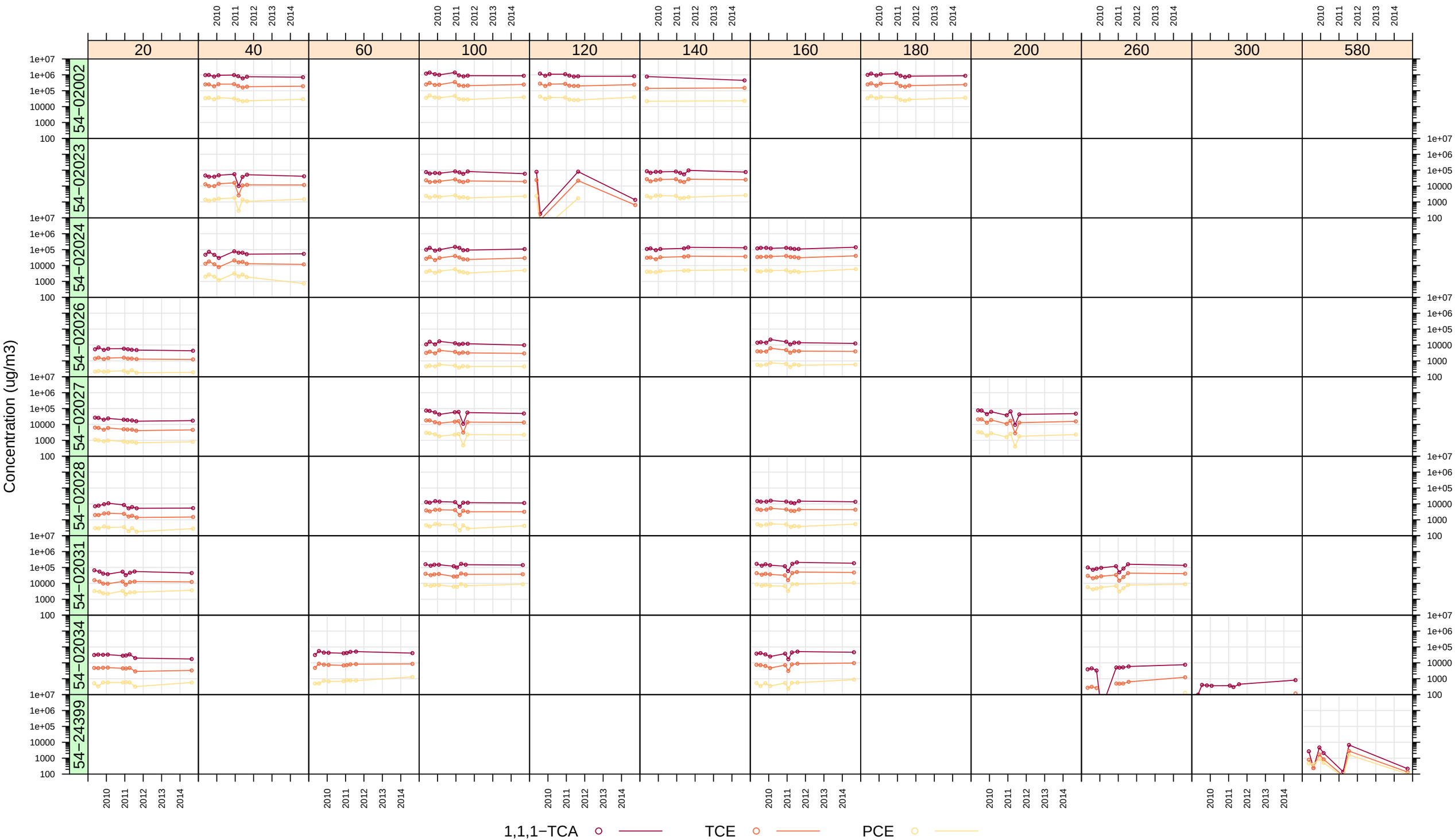

Figure 3−21

Recent Time History of VOC Daughter Compounds Within the Source Areas

Port Depth (feet bgs) and Year

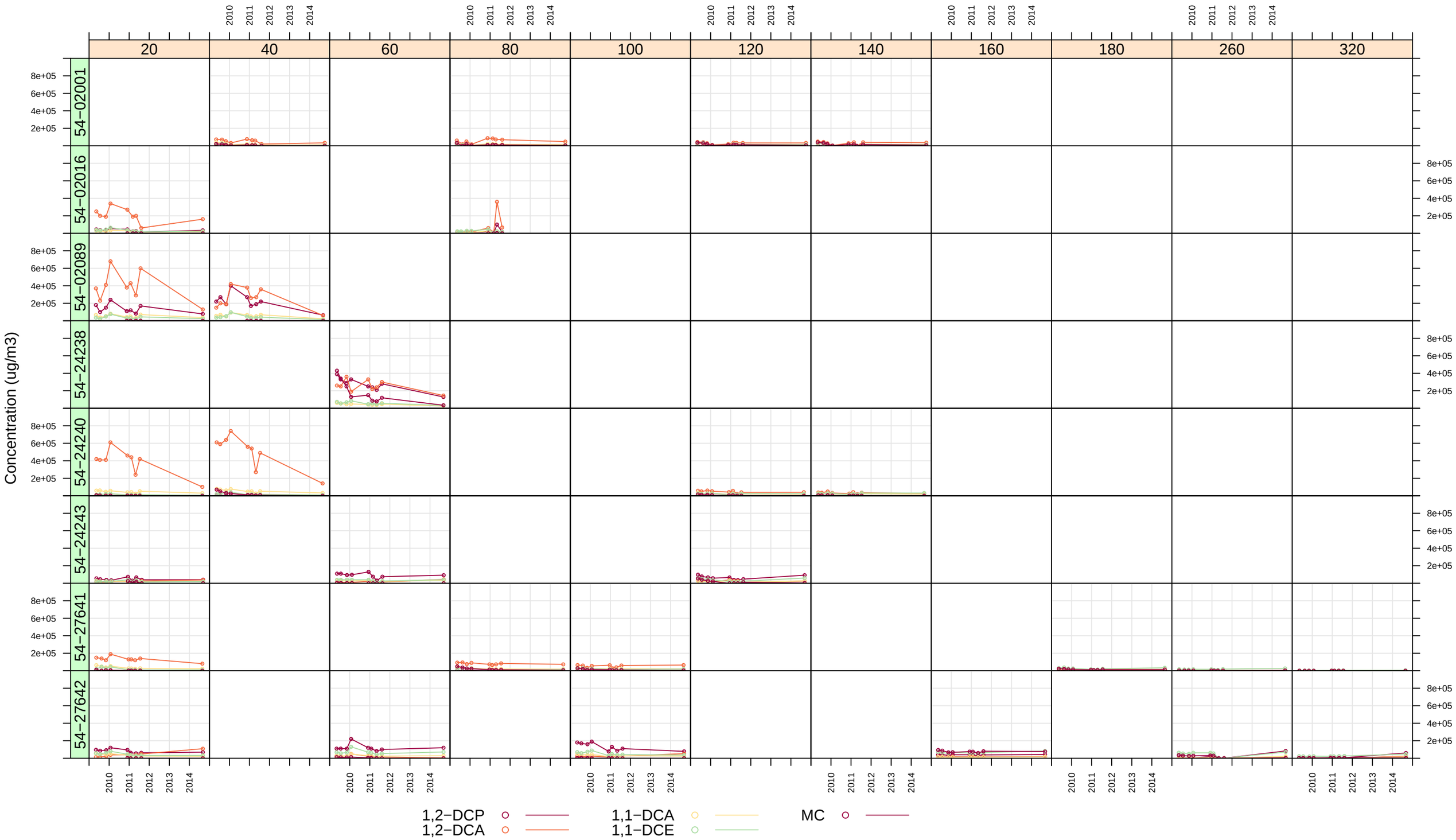

Figure 3−22

Recent Time History of VOC Daughter Compounds Within the Inner Plume

Port Depth (feet bgs) and Year

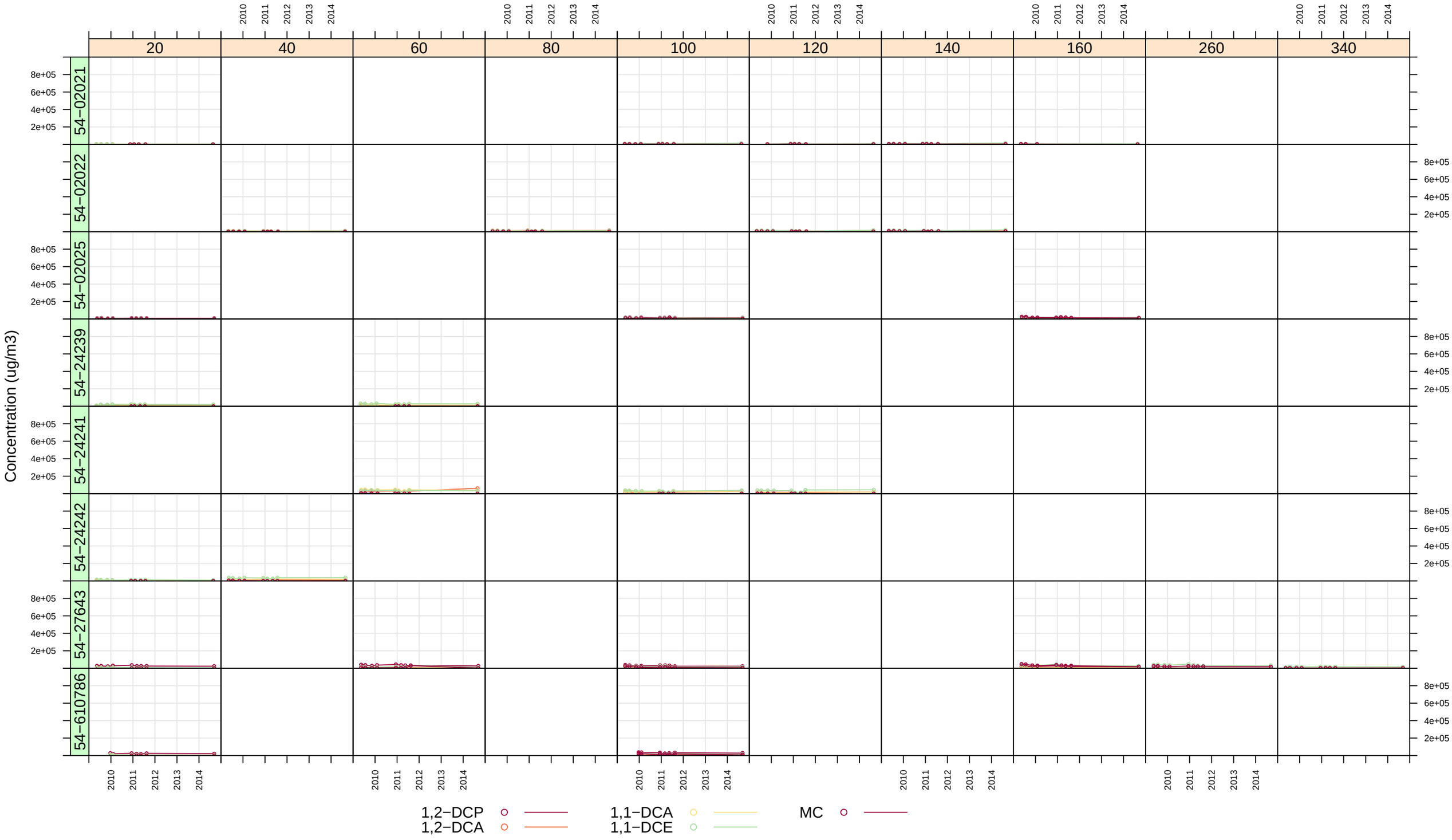

Figure 3−23

Recent Time History of VOC Daughter Compounds at the Plume Margins

Port Depth (feet bgs) and Year

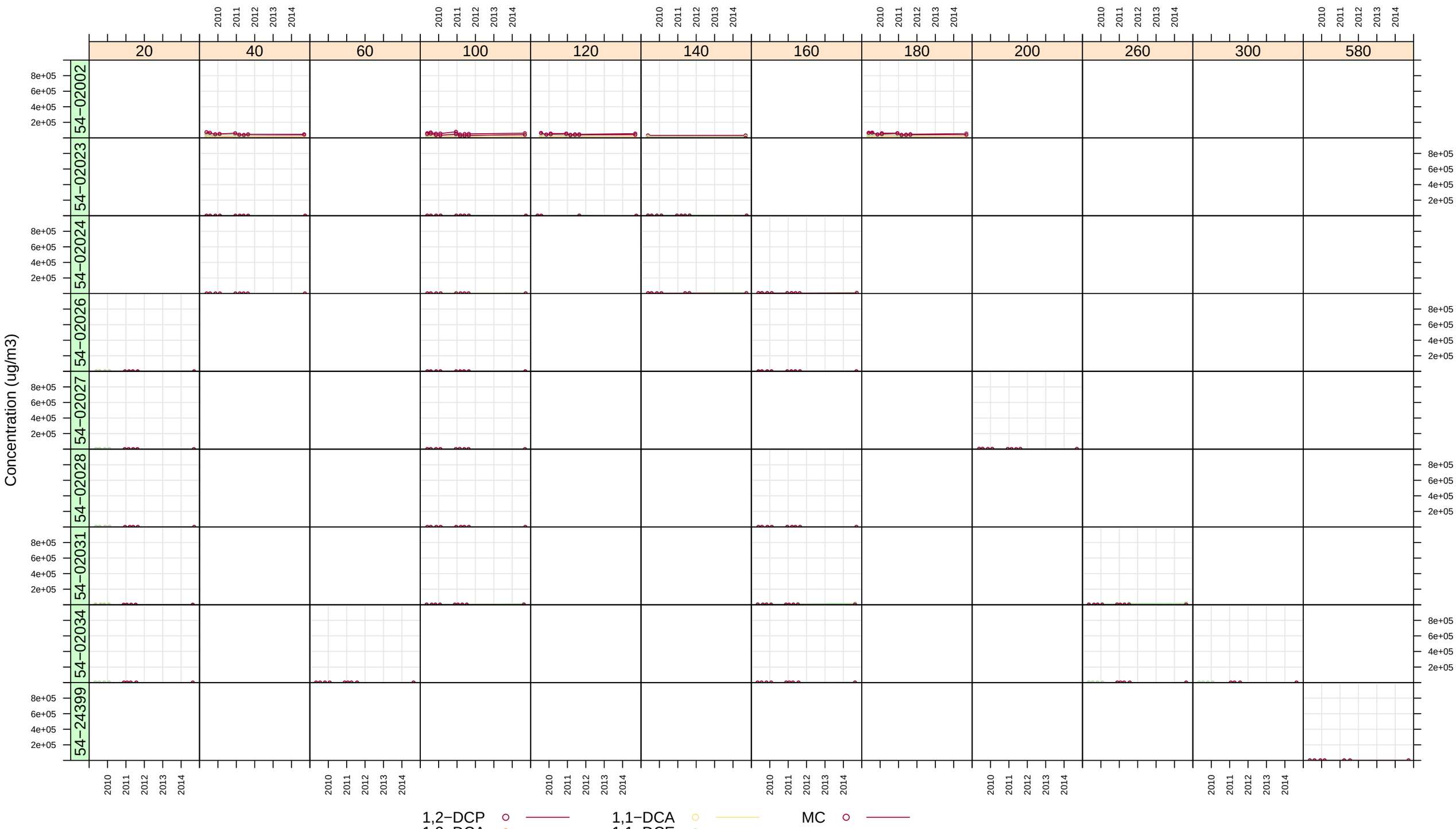

Figure 3−24

Recent Time History of VOC Daughter Compounds Within the Source Areas (log scale)

Port Depth (feet bgs) and Year

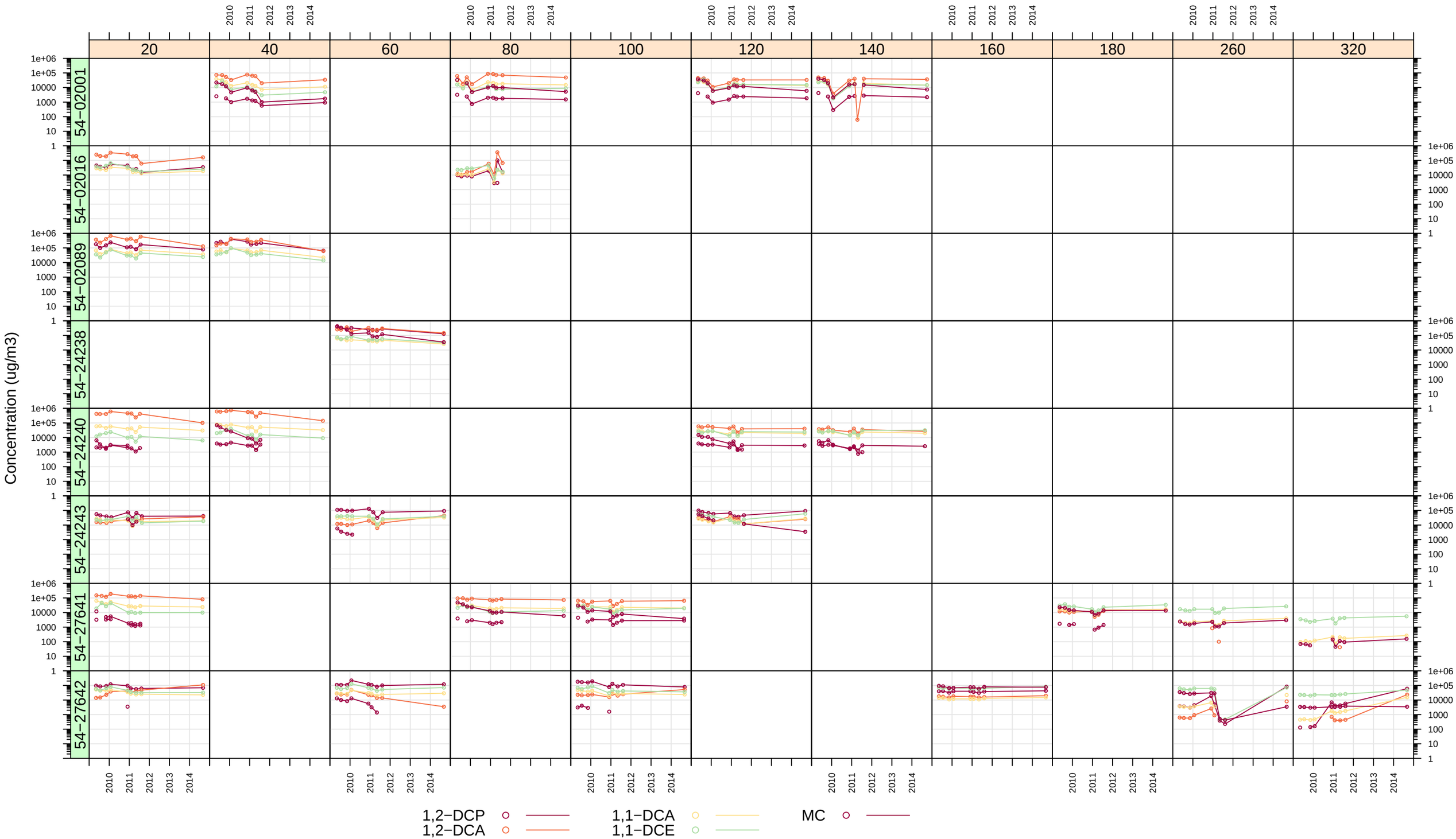

Figure 3−25

Recent Time History of VOC Daughter Compounds Within the Inner Plume (log scale)

Port Depth (feet bgs) and Year

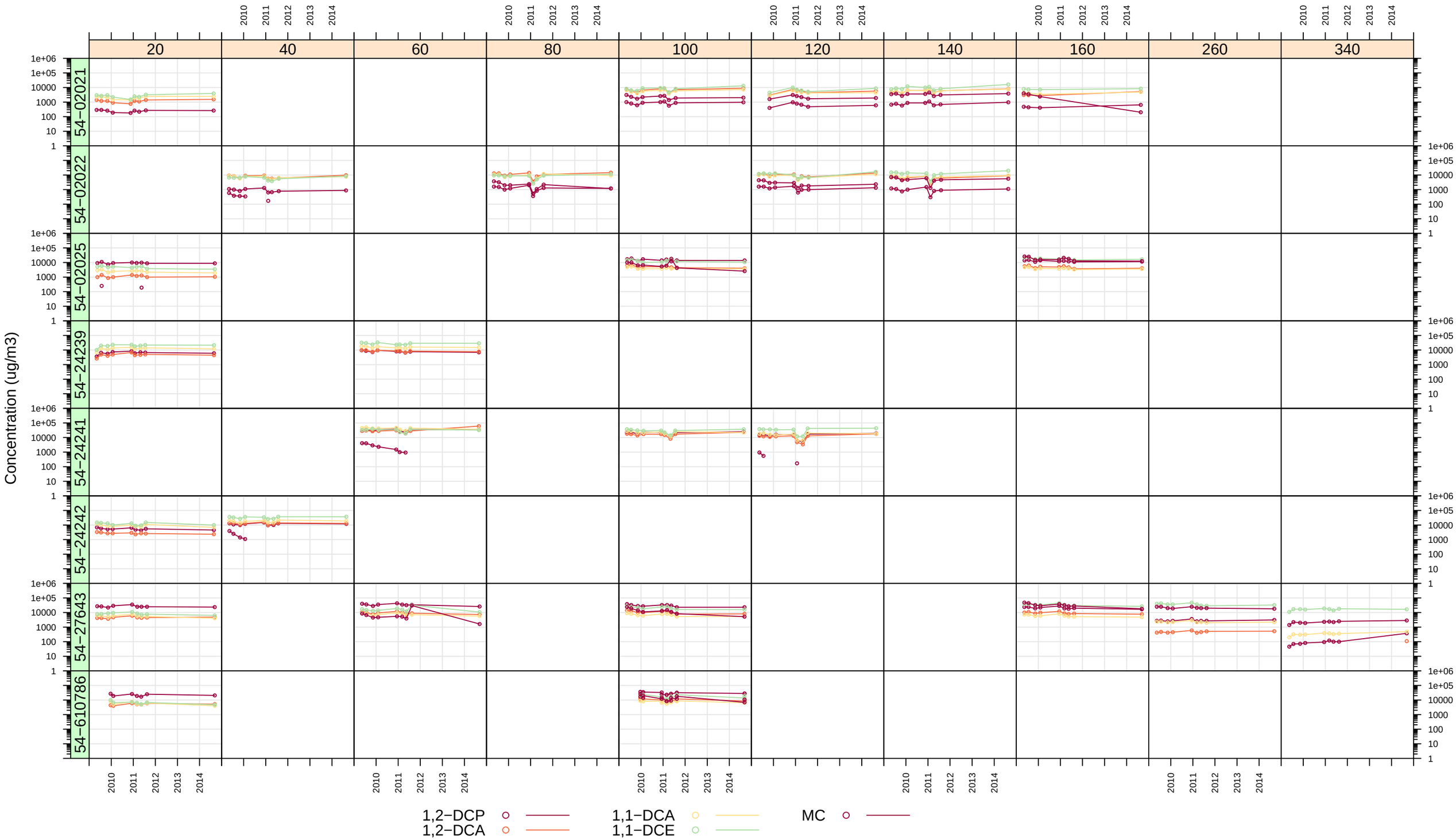

Figure 3−26

Recent Time History of VOC Daughter Compounds at Plume Margins (log scale)

Port Depth (feet bgs) and Year

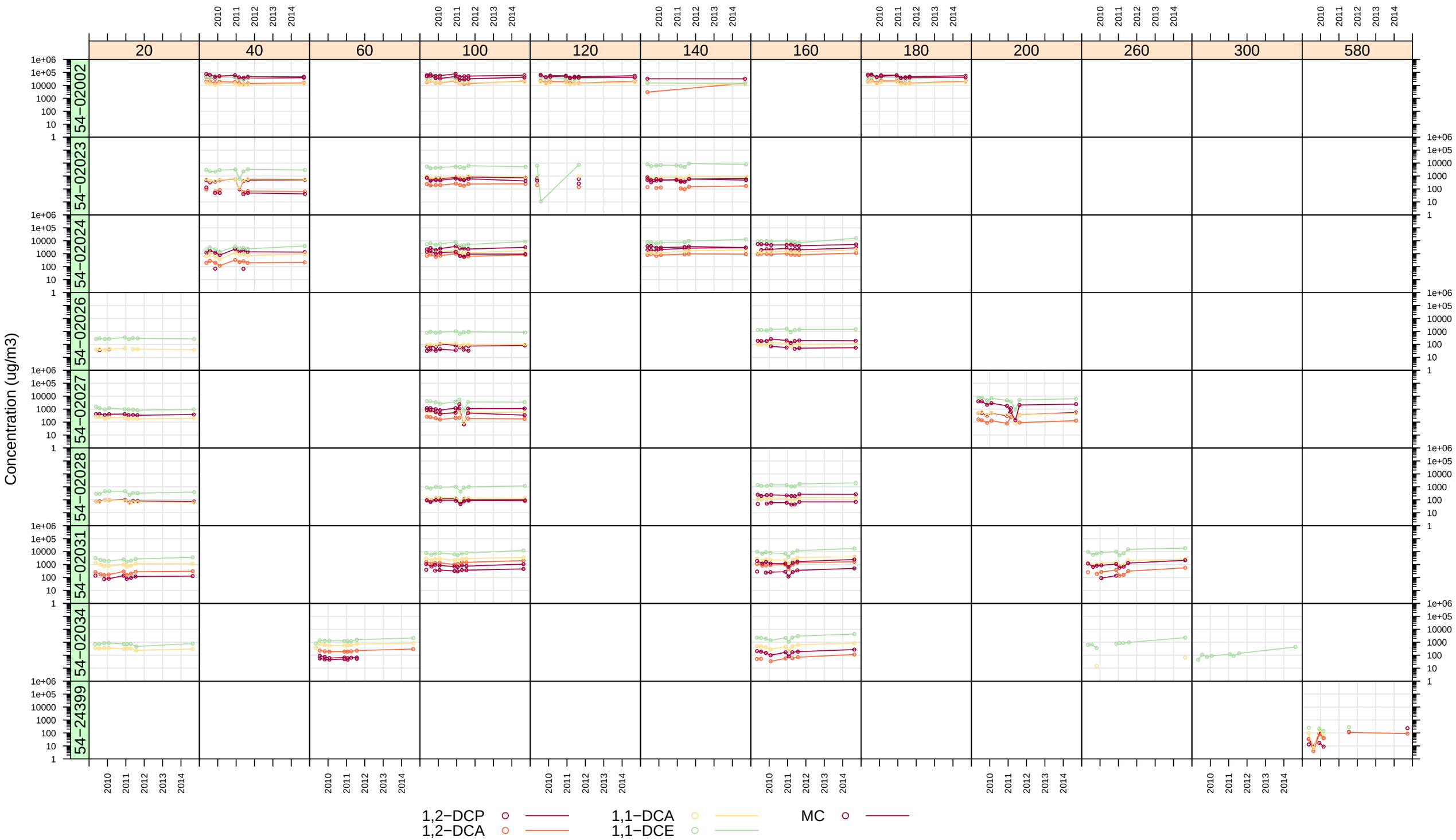

Table 2-1
Geologic Zone Characteristics

Geologic Zone	Porosity	Volumetric Water Content[a]	Air-filled Porosity	Bulk Density (g/cm^3)
Overburden	0.4	0.05	0.35	1.5
Qbt2	0.41	0.02	0.39	1.4
Qbt1vu	0.49	0.01	0.48	1.2
Qbt1vc	0.49	0.1	0.39	1.1
Qbt1g	0.46	0.08	0.38	1.2
Qbtt	0.45	0.14	0.31	1.2
Qct	0.45	0.14	0.31	1.2
Qbof	0.44	0.11	0.33	1.2
Qbog	0.67	0.2	0.47	0.8
Tpf	0.45	0.14	0.31	1.2
Tb4	0.001	0.0005	0.0005	2.7

[a] 2009 report "Moisture Monitoring at Area G, TA-54" and edits by Kay Birdsell

Table 3-1
Q4FY14 Contaminant Mass Distribution

Analyte (Tier1 ug/m^3)	*Strata*	*Tier1 Multiple*	*Contaminant Mass (kg)*				*% of Total Mass Within SVE ROI* [a]		
			Vapor	*Aqueous*	*Sorbed*	*Total*	*West*	*East*	*Total*
1,1,1-TCA (42,300)	Within Tshirege	>10x	231	43	23	296	6	17	23
		1x - 10x	221	43	23	287	5	1	5
	Total Within Tshirege		452	86	45	583	11	18	**28**
	Below Tshirege	>10x	22	12	3	37	0	3	3
		1x - 10x	70	38	13	120	1	3	4
	Total Below Tshirege		91	50	15	157	1	6	7
1,1,1-TCA Total			543	136	61	**740**	12	23	35
TCE (2,000)	Within Tshirege	>10x	165	53	41	258	14	19	32
		1x - 10x	7	2	2	11	0	0	0
	Total Within Tshirege		172	55	42	269	14	19	**32**
	Below Tshirege	>10x	26	25	10	61	1	6	7
		1x - 10x	3	3	3	9	0	0	0
	Total Below Tshirege		29	29	12	70	1	6	7
TCE Total			201	83	55	**339**	15	24	39

[a] SVE ROI is approximated as 125-ft within the Tshirege by LANL scientists.

Table 3-2
Contaminant Mass Uncertainty Analysis

Analyte	*Tshirege*	*Lower Confidence*			*Best Estimate*	*Mean*	*Upper Confidence*		
		95%	*80%*	*65%*			*65%*	*80%*	*95%*
		Contaminant Mass in kg							
1,1,1-TCA	Within	458	521	560	583	594	627	666	734
	Below	86	112	129	157	143	157	174	205
1,1,1-TCA Total		544	633	689	740	737	784	841	939
TCE	Within	202	233	252	269	267	283	301	334
	Below	39	49	56	70	61	67	74	86
TCE Total		241	282	308	339	329	350	375	419
		% Difference from Best Estimate							
1,1,1-TCA	Within	-21	-11	-4	0	2	8	14	26
	Below	-45	-28	-18	0	-9	1	11	31
1,1,1-TCA Total		**-26**	-14	-7	0	0	6	14	**27**
TCE	Within	-25	-13	-6	0	-1	5	12	24
	Below	-45	-31	-21	0	-13	-5	5	22
TCE Total		**-29**	-17	-9	0	-3	3	10	**23**

Table 3-3
Comparison of Total Contaminant Mass Among Sample Rounds

Total Contaminant Mass (kg)

Analyte (Tier1 ug/m³)	*Strata*	*Tier1 Multiple*	*Sample Round*					*% of Total Mass Within SVE ROI [a]*				
			Q1FY11	*Q2FY11*	*Q3FY11*	*Q4FY11*	*Q4FY14*	*Q1FY11*	*Q2FY11*	*Q3FY11*	*Q4FY11*	*Q4FY14*
1,1,1-TCA (42,300)	Within Tshirege	>10x	421	277	179	355	296	28	23	19	28	23
		1x - 10x	270	271	303	286	287	3	8	12	5	5
	Total Within Tshirege		691	549	483	641	583	31	31	31	32	**28**
	Below Tshirege	>10x	6	0	0	0	37	1	0	0	0	3
		1x - 10x	90	72	47	65	120	3	4	3	3	4
	Total Below Tshirege		97	72	47	65	157	4	4	3	3	7
1,1,1-TCA Total			788	621	530	706	**740**	35	35	34	35	35
TCE (2,000)	Within Tshirege	>10x	267	200	179	235	258	34	33	34	34	32
		1x - 10x	10	12	12	12	11	0	0	0	0	0
	Total Within Tshirege		278	211	191	247	269	34	33	34	34	**32**
	Below Tshirege	>10x	37	26	13	19	61	4	4	2	2	7
		1x - 10x	8	8	9	9	9	0	0	1	0	0
	Total Below Tshirege		45	34	22	28	70	4	4	3	3	7
TCE Total			323	245	213	274	**339**	38	37	37	37	39

% Difference from Q4FY14

Analyte (Tier1 ug/m³)	*Strata*	*Tier1 Multiple*	*Sample Round*					*Change in % of Total Mass Within SVE ROI [a]*				
			Q1FY11	*Q2FY11*	*Q3FY11*	*Q4FY11*	*Q4FY14*	*Q1FY11*	*Q2FY11*	*Q3FY11*	*Q4FY11*	*Q4FY14*
1,1,1-TCA (42,300)	Within Tshirege	>10x	42	-6	-40	20	0	5	1	-4	5	0
		1x - 10x	-6	-5	6	0	0	-2	2	7	0	0
	Total Within Tshirege		**19**	**-6**	**-17**	**10**	0	**3**	**3**	**3**	**4**	**0**
	Below Tshirege	>10x	-83	-100	-100	-100	0	-3	-3	-3	-3	0
		1x - 10x	-24	-40	-60	-46	0	0	0	-1	-1	0
	Total Below Tshirege		**-38**	**-54**	**-70**	**-59**	0	-3	-3	-4	-4	0
1,1,1-TCA Total			**7**	**-16**	**-28**	**-5**	0	0	0	-2	0	0
TCE (2,000)	Within Tshirege	>10x	4	-23	-31	-9	0	1	1	2	2	0
		1x - 10x	-8	5	7	4	0	0	0	0	0	0
	Total Within Tshirege		**3**	**-22**	**-29**	**-8**	0	**1**	**1**	**2**	**2**	**0**
	Below Tshirege	>10x	-39	-58	-79	-69	0	-3	-3	-5	-4	0
		1x - 10x	-13	-6	0	-1	0	0	0	0	0	0
	Total Below Tshirege		**-36**	**-51**	**-69**	**-60**	0	-3	-3	-4	-4	0
TCE Total			**-5**	**-28**	**-37**	**-19**	0	-1	-2	-2	-2	0

[a] SVE ROI is approximated as 125-ft within the Tshirege by LANL scientists.

Appendix C: Accessing Hidden Features of Figures 3-1 Through 3-10

This appendix contains instructions for navigating the hidden features embedded in the digital copies (i.e. the portable document format (pdf) by Adobe) of Figures 3-1 through 3-10. These 10 pages contain layers that can be toggled on and off as well as clickable objects that yield sample attributes and results without having to refer to Appendix A for the actual data.

The pdf layers are accessed using the "layers panel", which should be visible on the left-hand side of the Adobe instance. If it is not, it can be opened using the icon on the ribbon at the far left. Once open, a single step should be performed within the layers pane to make subsequent navigation easier. Figure 1a below is a partial view of the page list with embedded layers. These list items are actually layer groups associated the pages. The icon should be clicked and the "List Layers for Visible Pages" option should be selected (see Figure 1b) to hide all layer groups except the one associated with the active page. This will eliminate confusion later when the user has changed pages and wants to toggle between layers. Clicking the icon expands the group for the active page to expose the actual layers (Figure 1c) and this step only needs to be performed the first time a page accessed. The visible layers have an icon and the invisible layers have an icon. The only layers not visible by default should be those inside the "Report Contours" layer, which can be expanded using the icon. The layer status from the active page is carried over when the user changes pages to facilitate comparisons of different views among the various pages.

Figure 1a

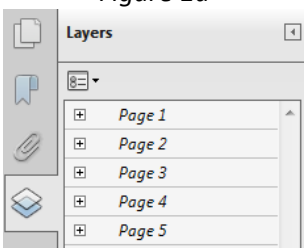

Figure 1b

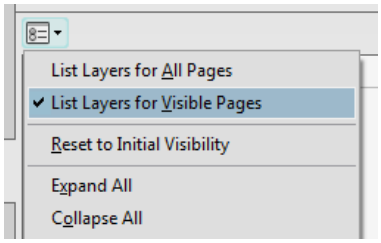

Figure 1c

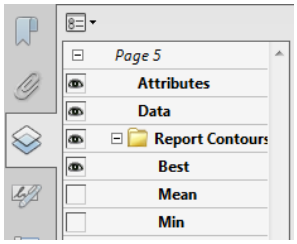

The "attributes" layer contains "object data" that can be used to obtain concentrations of several analytes and other sample attributes such as depth and geologic zone. The object data are obtained using the "object data" button on the "analyze" toolbar, which is highlighted here . Clicking this icon causes the mouse pointer/hand icon to become a crosshair icon when hovering over a feature (the sample points in this case) containing object data. Clicking a feature brings up the "model tree" panel (Figure 2), which is divided into three panes that can be adjusted using the handles that are highlighted. After viewing object data, the layers panel can can be re-activated using the icon. The object data may only be accessed when the "sample attributes" layer is on.
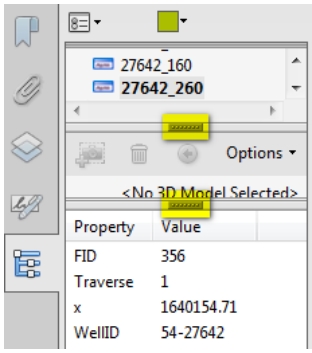
Figure 2